

**POLY-DIMETHYL-SILOXANE BASED RESPONSIVE
STRUCTURES**

A Thesis
Presented to
The Academic Faculty

by

Brian Kwong

In Partial Fulfillment
of the Requirements for the Degree
M.S. in the
School of Mechanical Engineering

Georgia Institute of Technology
DECEMBER 2014

COPYRIGHT 2014 BY BRIAN KWONG

POLY-DIMETHYL-SILOXANE BASED RESPONSIVE STRUCTURES

Approved by:

Dr. Kyriaki Kalaitzidou, Advisor
School of Mechanical Engineering
Georgia Institute of Technology

Dr. Karl Jacob
School of Materials Science and
Engineering
Georgia Institute of Technology

Dr. Alexander Alexeev
School of Mechanical Engineering
Georgia Institute of Technology

Dr. Antonia Antoniou
School of Mechanical Engineering
Georgia Institute of Technology

Date Approved: August 2014

ACKNOWLEDGEMENTS

I want to express my gratitude and thanks to all the people whose help and support made this work possible. In particular, I want to specially thank Professor Kalaitzidou, my advisor for taking the time to educate me and allowing me to grow under her tutelage. Without her support and guidance I would not be the person I am today.

I also want to thank my friends in the lab for their collaboration throughout the past two years. This graduate school experience would have been a struggle if I wasn't in such an accepting group. Therefore it is my great pleasure to thank and acknowledge Atiq, Mehdi, Sanzida, and Erin. I would also like to acknowledge the help from Neel and Jordan with fabrication of the structures and Drew for help with magnetic actuation and PDMS processing. To my friends and family outside the lab please accept my thanks for providing me the much needed anchor to the real world.

I would like to acknowledge NSF for funding from two grant programs. The first is award number 1256403 under the direction of Professor Alexeev and award number 1301268 under the direction of Professor Antoniou.

Finally, I want to thank my parents, Salina and Kelvin, for all their assistance and love. I am forever grateful and indebted for everything they have given me.

TABLE OF CONTENTS

Acknowledgements.....	iii
List of Tables	v
List of Figures.....	vi
Summary.....	vii
Chapter 1. Introduction.....	1
1.1 Smart Materials	1
1.1.1 Silicone Elastomers.....	4
1.1.1.2 Actuation of PDMS Structures	8
1.2 Artificial Cilia	17
1.3 Nanoporous (NP) Metal Foams	21
1.4 Thesis Goal and Objectives.....	24
Chapter 2. PDMS Composite Cilia Arrays.....	26
2.1 Design.....	26
2.2 Materials selection.....	31
2.3 Fabrication Method	31
2.3.1 Mold fabrication.....	32
2.3.2 Casting	36
2.4 Characterization of cilia arrays	38
2.4.1 Shape and geometry	38
2.4.2 Dispersion and Distribution of Fe-particles within the PDMS matrix	40
2.4.3 Modulus Measurement.....	45
2.5 Magnetic actuation of cilia arrays	46
2.6 Alternative approach to create tilted cilia	47
2.7 Conclusions	49
Chapter 3. Laminated composites with PDMS and Nanoporous (NP) Metal Foams ..	51
Chapter 4. Conclusions and Suggestions for Future Work	59
4.1 Results	59
4.2 Future work	59
References	62

LIST OF TABLES

Table 1: Average fluid velocity based on bend angle, columnar aspect ratio of 7, elastic modulus of 1 MPa.....	30
--	----

LIST OF FIGURES

Figure 1-1: Classification of stimuli of responsive materials[8]	1
Figure 1-2: Process sequence for fabricating PDMS stamps [23]	5
Figure 1-3: Bending of pillars, aspect ratio of 4, fabricated using dry embedding [36]... ..	11
Figure 1-4: Schematic representation of “strain engineering” manufacturing method [40]	12
Figure 1-5:a) Shape transition triggered by temperature. b) Alignment of particles in forced flow, top; and random flow bottom [1]	13
Figure 1-6: Wrinkles formed from pre stretching PDMS prior to Au deposition [42].....	14
Figure 1-7: Schematic of a strained bilayer film folding into a tube when W is large, but into a coil when W is small. The arrows indicate the folding direction[39].....	16
Figure 1-8(a) Lung cilia [52] (b) sensory cilia on a spider leg [53]	18
Figure 1-9: Photolithography Process Sequence for Rectangular Magnetic Cilia [57] where f shows the released structure	19
Figure 1-10: Simulation of cilia array for particle deposition and removal[61] , Cilia tilted along fluid flow (top) and against (bot)	21
Figure 1-11: SEM micrograph of nanoporous Au [74]	23
Figure 2-1: (a) Laser confocal image of su8 mold, (b) Height profile of cross section....	33
Figure 2-2: Laser cut acrylic mold.....	34
Figure 2-3: PDMS pillars made from laser cut Kapton mold.....	35
Figure 2-4: Fabrication process for the PDMS column structure (a) Acrylic mold fabrication, (b) PDMS/Fe mixture, (c) Pillar Array fabrication	37
Figure 2-5: Released 40wt% Fe-PDMS pillars.....	38
Figure 2-6: Representative images of (a) top and (b) bottom surfaces of the laser cut acrylic mold	39
Figure 2-7: Representative image of polymer columns.....	40
Figure 2-8: Representative cross section of PDMS/FE composite.....	42
Figure 2-9: Particle aggregate size distribution for 20Wt % Fe	43
Figure 2-10: Particle aggregate size distribution for 30Wt % Fe	44
Figure 2-11: Particle aggregate size distribution for 40Wt % Fe	44
Figure 2-12: DMA measured elastic modulus	45
Figure 2-13: Neodymium magnetically actuated pillars: (a) 20Wt%, (b) 30Wt%, and (c) 40Wt% concentration.....	46
Figure 2-14: Fabrication process for sandwich structures	48
Figure 2-15: Sandwich Structure	49
Figure 3-1: Fabrication process for polymer/foam bi-layer (a) PDMS film fabrication (b) Pre-stressed bilayer fabrication.....	53
Figure 3-2: Thickness vs Spin Speed calibration curve.....	55

SUMMARY

This thesis focuses on the design, fabrication and characterization of polymeric smart structures that are able to alter their geometry and thus their properties upon the application of external stimuli in a reversible and controllable manner. Two different responsive structures are studied that both contain poly dimethyl-siloxane (PDMS) and differ in the design, geometry, and actuation mechanism. The first structure is a surface decorated by a square array of posts (cilia) made of PDMS reinforced with magnetic particles and is actuated magnetically. The structures are meant to mimic cilia, a hair-like structure found in nature. The physical parameters necessary for the magnetic response of the cilia including physical dimensions and filler concentration are investigated. In addition, the elastic modulus of the composites is measured and the microstructure is examined in order to determine the dispersion and homogeneity of the composites. The second structure is a planar hetero-structure consisting of a PDMS substrate and a nanoporous (NP) metal foam film which is actuated thermally or chemically by tuning the generation and release of residual stresses at the NP metal foam/PDMS interface. The effect of strain, applied to the PDMS substrate prior to the deposition of the NP metal foam and the effect of the PDMS and NP metal foam thicknesses on the shape/size of the planar hetero-structure after the actuation is investigated.

Chapter 1. Introduction

1.1 Smart Materials

Smart materials are materials that can respond in a controlled and reversible manner to external stimuli such as temperature[1, 2], electric field[3], magnetic field[4, 5], pH [6]and light[7]. The actuation happens due to the generation and release of stresses within the material upon the application of the trigger [8-10]. A classification of smart materials based on the corresponding stimuli is shown in the schematic of Figure 1-1.

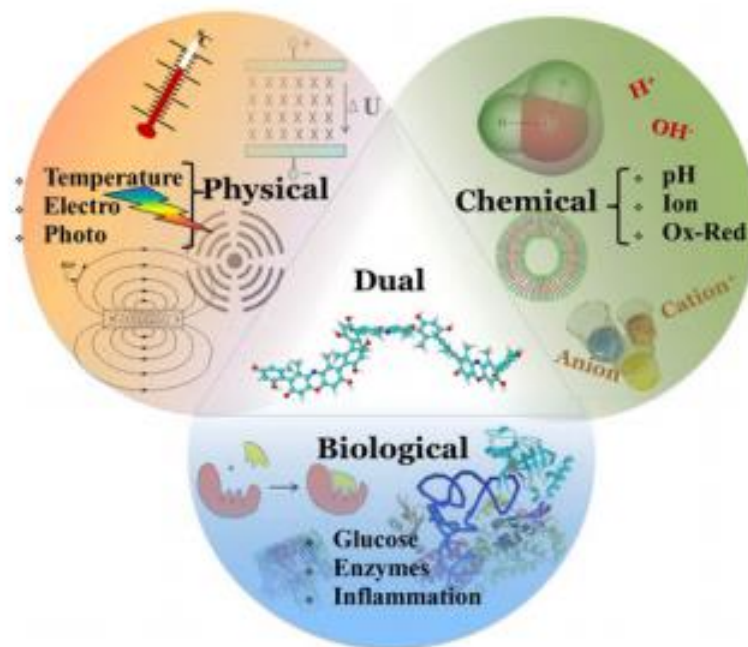


Figure 1-1: Classification of stimuli of responsive materials[8]

A very common smart material/structure is the thermostat, a bimetallic strip that bends upon heating/cooling due to differences in the coefficient of thermal expansion of the metals making up the strip. Other applications for smart materials include self-healing, intelligent sensors, actuators, filtering, and artificial muscles. Smart structures can be made using various materials such as shape memory alloys [11], shape memory polymers[12],

piezoelectric materials [13], and/or hetero-structures [14] that consist of more than one material type. Smart structures can span various length scales from nano-scale i.e, artificial muscle fibers [15] to macro-scale i.e, bars for vibration isolation of bridges[16].

Of interest are the stimuli responsive polymers, which fall into two different categories. The first category consists of polymers that undergo a physiochemical change including changes to hydrophobicity, bond cleavage, solubility, and degradation [8] upon application of a trigger. The second category the polymer is made responsive by incorporation of various fillers/reinforcements i.e, particles with electric or magnetic properties, which is also the primary focus of this thesis.

Polymer brushes and shape memory polymers (SMP) belong to the first category. Numerous polymers and fabrication methods are used to create stimuli responsive polymers. A method to create polymer brushes is grafting responsive material onto the substrate to create a stimuli responsive surface. The new composite is now functionalized by the newest additional layer on the primary substrate. “Grafting-to” and “grafting from” are the two basic methods used for this type of fabrication. In “grafting-to” end functional polymer chains react with the surface to form bonded layers while in “grafting-from” the polymer is synthesized on the substrate [17]. This idea can be extended to creating new composite materials through the attachment of reactive materials onto the surface of other solid substrates. SMP is a well-researched field within smart materials with studies conducted to examine the response of modified SMP on various stimuli. SMP are polymers that switch from a temporary state back to the permanent original state. The basic requirement for SMP is a stable polymer network which dictates the original state and a reversible switching transition. Commercial SMP have been developed from polyurethane,

polystyrene, aliphatic polyurethane, and even an epoxy based resins [18]. Both regular polymers and SMP are restructured with various composite methods in order to strengthen, add, and/or modify their stimuli responses.

Fillers/reinforcements that are mixed into polymers to add responsiveness to external stimuli include electrically conductive materials, such as carbon fibers, carbon nanotubes and graphite [19], piezoelectric materials such as barium titanate [20], thermally conductive materials such as boron nitride [21] and magnetic materials including metal particles, iron(III) oxide, and nickel powders [22]. Light stimuli have also been added by using chemicals that form photo-induced reversible crosslinks. Mechanical mismatch between two materials, formed by a SMP laminated to an elastic polymer [18], has also been used as a way of creating a SMP composite.

As mentioned above, there are numerous polymers and fabrication methods used to create smart materials and structures. The focus here is on polymer composites, specifically the second category mentioned, with emphasis on two different designs. A thermoset elastomer, polydimethylsiloxane (PDMS) will be used in both designs. One case will have the PDMS be reinforced with magnetic particles (filled composites) and a magnet will be used to trigger the response. In the second case, PDMS layers will be bonded to metallic foams creating a planar hetero-structure (laminated composites) and the trigger will be temperature which will actuate the structure due to the differences in the coefficient of thermal expansion of the two layers. In both cases, the response is reversible, with the structures going back and forth between the two states by reversing the trigger. This is due to the generation and controlled release of residual stresses in the composites. In addition to investigating the effects of filled versus laminated composites on the response, this

research also investigates the shape of the structures. The filled composite will be shaped as a surface decorated with an array of cilia (posts) while the laminated structure will be a planar surface.

1.1.1 Silicone Elastomers

Elastomers, a subset of polymers, possess significant viscoelasticity which make them ideal base materials for deformable composite materials. In particular, silicone elastomers are commonly used in industry as these materials are generally non-reactive and many can easily withstand temperatures in the order of 150°C. Polyurethanes, polyimides, and silicone rubbers are examples of elastomers with PDMS one of the most commonly used silicone rubber since the late 1990s mainly due to its great adhesive properties and easily tunable mechanical properties than make it a very versatile material.

1.1.1.1 Fabrication of PDMS Structures

PDMS is a thermoset polymer that is composed of a monomer and a hardener. By tuning the ratio of the two materials and the curing conditions, one can modify the elastic modulus of the polymer. The standard ratio of monomer to hardener is 10:1. Many different fabrication techniques with this material have been developed over the years with many found under the umbrella of soft lithography.

Soft lithography refers to a set of techniques that utilize “patterned elastomers as the stamp, mold, or mask (rather than a rigid photomask) to generate micropatterns and microstructures” [23]. Techniques under this broad umbrella include microcontact printing, replica molding, microtransfer molding, micromolding in capillaries, solvent-assisted micromolding, embossing, and cast molding [23]. Note that in most cases the PDMS molds used with soft lithography were fabricated through cast molding. The process for fabrication of the PDMS molds is demonstrated in Figure 1-2.

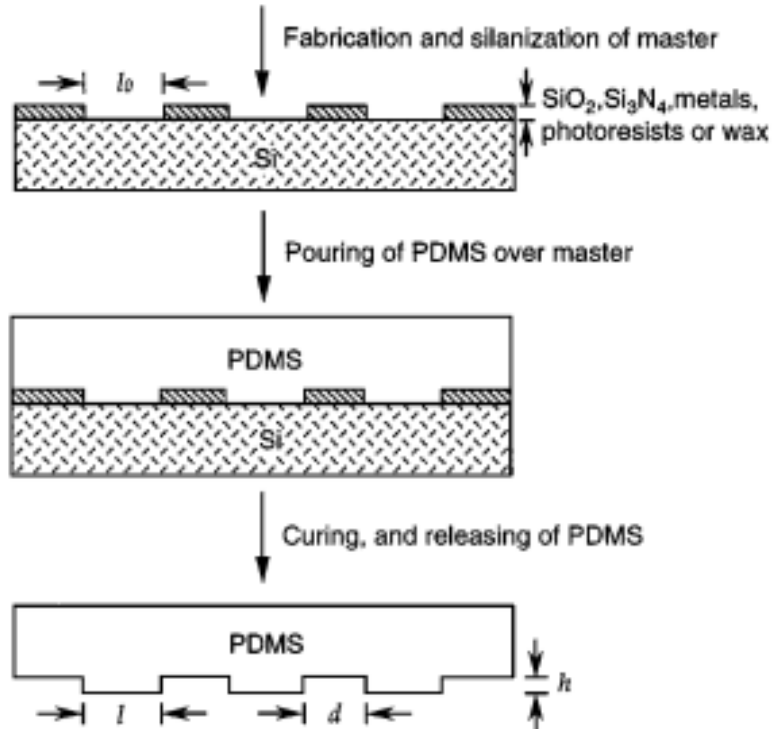


Figure 1-2: Process sequence for fabricating PDMS stamps [23]

Microcontact printing utilizes the surface of a PDMS pattern to transfer patterns of self-assembled monolayers on the substrate through contact. The technique relies on the rapid formation of the monolayer and that the monolayer will effectively block itself from spreading. This technique can then be used as an etch mask for certain wet etching and as template for deposition of other materials [23].

Replica molding utilizes the PDMS as mold material rather than using a rigid material mold to duplicate the 3-d mold topography in a single casting step. This enables the replication of smaller and more fragile structures. Microtransfer molding uses a PDMS mold for replica molding rather than the original master mold; the mold is filled with the prepolymer and then placed in contact with a substrate. Subsequent curing of the polymer and removal of the PDMS mold yields the desired microstructure on the substrate.

Micromolding in capillaries uses the PDMS mold to form an array of empty channels that is filled through capillary action [23].

Solvent assisted micromolding uses the PDMS mold to hold solvent of the substrate material. When the PDMS mold is pressed into the substrate surface, the solvent dissolves parts of the substrate and the resulting fluid is molded against the PDMS. This is similar to embossing, where a mold is heated and pressed into a substrate to imprint the desired structure, with the heat softening the substrate. Cast molding is pouring an uncured polymer over top of a master relief structure with the final structure coming into shape after curing and removal of the polymer from the initial master [23].

Master mold fabrication can be done through either building up the structure from the substrate or through material removal from the substrate. Generally photolithography or material removal techniques are employed in making the master mold. Molds made by photolithography are typically either made from or patterned with a photoresist, which is either hardened (negative) or rendered soluble (positive) by UV light [24].

The same mask pattern can then be used to create either the structure or the relief of the structure in the photoresist. A single step fabrication process would cure the resist so it is a relief of the desired structure. A multi-step option, more closely in line with replica molding, would cure the initial master in the desired structure shape. This master structure is then utilized to fabricate a second mold that is the negative. The choice of method is dependent on the structure size and mold material type as there are limitations to the resolution of each type of photoresist.

Material removal techniques machine the substrate into the correct shape rather than surface machining the desired features. Variations of this technique include chemical

etching, laser cutting, and manual puncturing of polymer sheets. In many cases, these removal procedures are serial rather than the batch fabrication of photolithography.

Chemical etching relies on the same processes as photolithography to determine feature shapes so it is considered a batch process. In many cases, the molds would be fabricated on Si wafers due to large array of chemicals that can be utilized to fabricate the desired shapes. Chemical etching along with plasma techniques can create high aspect ratio features, due to techniques like deep reactive ion etching which allows for near vertical sidewalls in silicon.

Laser drilling to create a mold is a very flexible process and well suited towards high aspect ratio fabrication. The range of materials that can be used for this process is very broad as the laser's power and wavelength can be tuned to remove most materials. Examples of materials being used in laser drilling are gold films[25], kapton film, and plastics like acrylic and PMMA[22]. The heating caused by the laser striking the mold however can potentially cause fabrication challenges, as localized heating will deform the surface features during cutting. This is readily apparent in cylindrical structures that end up cone shaped through this fabrication. Microdrilling, which uses a physical tool rather than light to create the holes, allows for smoother straight holes and more complex shape features, but takes more time.

A unique idea to fabricate molds on the microscale without the use of special equipment was to fabricate the molds out of biaxially oriented polystyrene thermoplastic sheets [26]. By cutting the shapes onto the sheet, or in one example, using needles to puncture the sheet [27], smaller features would be formed when the sheet is heated up. The sheets would shrink in-plane and expand out of plane, which needs to be accounted for in

the initial design of the holes placed in the material. However the limitation to this technique is the sheet thickness.

The above discussion clearly indicates the variety of methods that have been employed to fabricate patterned surfaces and complex geometry structures made of PDMS at various length scales. PDMS surfaces and structures have been used in various applications including but not limited to microfluidics, sensors, actuators, artificial muscles, and self-cleaning. Both the wide range of fabrication methods and the versatility of the PDMS as material are the main reasons for using PDMS in this study,

1.1.1.2 Actuation of PDMS Structures

PDMS structures have been used as actuators in a variety of applications using magnetic fields[4], electrostatic forces[3], temperature [1] and solvents as stimuli [6].In this thesis, magnetic field actuation and stress based actuation, where the stress is generated due to changes in temperature, are the primary actuation methods.

Magnetic actuation in elastomers has been pursued with the creation of magnetic composite polymers manifesting magnetic susceptibility. These materials are formed by introducing magnetic filler particles into a polymer matrix and share similarities with ferrofluids and other magnetorheological materials. Magnetic materials are desired for actuation as magnetic forces can act at a distance and is not limited by the fluids it can be used in. A material's potential as a magnetic material is dictated by its magnetic susceptibility which indicates how much a material is magnetized in response to an applied magnetic field. Magnetic materials can be divided into five different classes based on their magnetic susceptibility: diamagnetism, ferromagnetism, antiferromagnetism, paramagnetism, and ferrimagnetism [28]. The focus here is on the more common type of positive magnetic susceptibility materials, paramagnetic and ferromagnetic materials.

Paramagnetic materials are materials that have a small and positive magnetic susceptibility. These materials are susceptible to applied magnetic field but do not retain the magnetic properties when the field is no longer applied. “Superparamagnetic” materials is a class of paramagnetic particles with a higher susceptibility. These materials typically have a nano size metal (or ferromagnetic material) core coated with a polymer [29] .

Ferromagnetic materials have a strong and positive magnetic susceptibility; as such these are the materials considered “magnetic” as they retain some of the magnetic properties after removal of the applied field. Ferromagnetic materials can be further classified as soft or hard. Soft magnetic materials are readily magnetized at low magnetic fields but tend to quickly lose their magnetization. Hard magnetic materials are not readily magnetized or demagnetized, so are ideal for permanent magnet applications. Of note is the alignment of the hard magnetic materials as these materials have defined magnetic poles.

Common soft magnetic materials used for magnetic composites are iron, nickel, cobalt and their respective alloys and oxides [30]. Some of these common materials are also coated to ensure that oxidation does not occur, which is different than “super paramagnetic” material. Magnetite and maghemite are examples of iron oxides that are prevalent and permalloy, a nickel and iron alloy, has also been used. Figure 1-3 shows a magnetically actuated structure fabricated with a soft magnetic material filler.

Rare earth magnets have also been utilized to create stronger magnetic composites. Hard barium ferrite powder, NdFeB, in PDMS were demonstrated as films [31] and in the fabrication of a micromixer [32]. The group at Simon Fraser University has demonstrated

similar filler magnetic material, specifically $(\text{Nd}_{0.7}\text{Ce}_{0.3})_{10.5}\text{Fe}_{83.9}\text{B}_{5.6}$, for use with PDMS [33, 34]. The concern with permanent magnet materials is their availability and the particle alignment.

The introduction of a stiffer material into the matrix comes with the consequence of stiffening the polymer. There is a limit to the amount of particles that are introducible to the polymer matrix. With too high particle content, the polymer will not cure and/or the elasticity of the polymer will be compromised significantly. In addition a large concentration of filler material may lead to agglomeration of the particles in the material rendering the material non-homogenous and the response in presence of the trigger non reproducible.

During fabrication of magnetic composites, an applied magnetic field can be used to manipulate the particles prior to curing. This would result in anisotropic composite materials. The magnetic particles will align in the field to form chains; as such there is an increase in reinforcement along the chain direction. Varga et al demonstrated the difference in material properties between a homogenous and an anisotropic Iron/PDMS composite [35]. They also demonstrated a strengthening effect when the magnetic composite material was placed in an external magnetic field. Anisotropic composite material can be fabricated by first embedding the mold with the magnetic particles prior to the addition of the polymer [22, 36]. This would concentrate the magnetic particles at the structure tip which would allow for more force to be directed further from the base. This would mean less material would be needed to bend the structure versus a homogeneously distributed magnetic composite. However, with enough magnetic powder the structure will be relatively homogenous after the polymer is added.

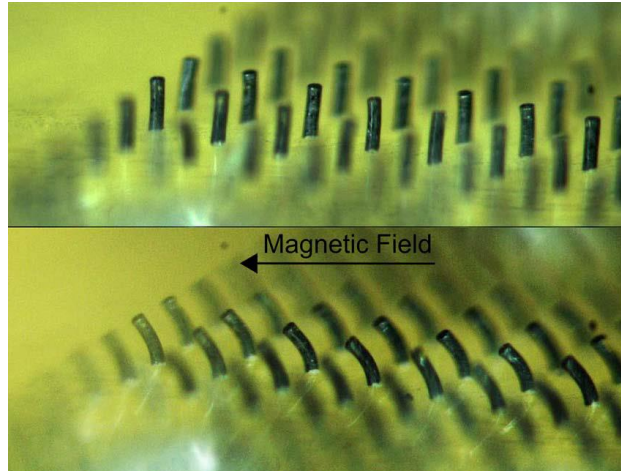


Figure 1-3: Bending of pillars, aspect ratio of 4, fabricated using dry embedding [36]

A smart structure can also be designed to respond due to the presence of intrinsic/residual stresses. For example a planar bilayer structure can bend due to the development of interfacial residual stress. This has been studied as a classical problem in mechanics with the basic principle used in a wide range of applications, including bimetallic strips in thermostats [37] and as a fabrication process for certain three-dimensional micro/nano-objects [38-40]. In these examples, strained planar heterostructures are grown or deposited layer by layer on a sacrificial substrate. When the structures are released from the substrate, due to the presence of lattice-misfit strain, they roll up to form freestanding three dimensional structures upon debonding. The idea of using strain engineering for fabrication of micro/nano-size objects is shown in Figure 1-4. The technology has been used to create rigid structures used as capacitors, building blocks for transistors, sensors and MEMS [41]. The method when used with most of the primary semiconducting or metallic materials leads to rigid three-dimensional objects. However, these structures are too rigid and cannot change their geometry or properties.

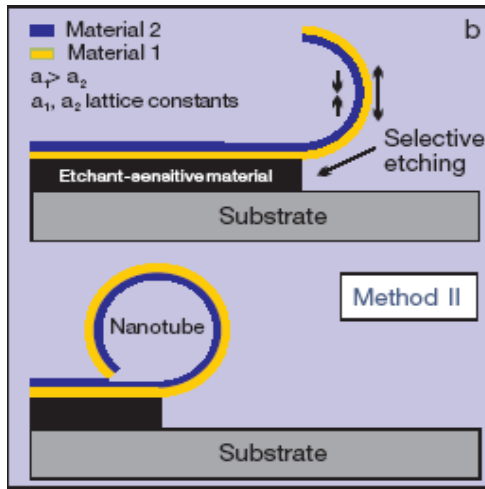


Figure 1-4: Schematic representation of “strain engineering” manufacturing method [40]

Recently strain engineering has been employed to manufacturing stimuli responsive particles with a cylindrical geometry[1]. A cylindrical geometry offers several advantages, as shown in Figure 1-5, compared to other shapes. A multiwall tubular geometry allows for high density packing (high surface to volume ratio) and upon unfolding increases the chance of potential formation of a percolating network. Thereby altering properties such as permeability and conductivity of the dispersing medium. Furthermore, due to their cylindrical shape and high aspect ratio, the particles can align in a flow field and be easily transported. With an elastic instability, a very small change in temperature causes a large change in shape as shown in Figure 1-5. Both the critical temperature value and the time scale, or speed of the shape transition, are directly related to the processing conditions used, the material properties and dimensions of the bilayer hetero-structures. The sensitivity and selectivity of the stimuli-response behavior is directly linked to the combination of material properties and the geometric design of the responsive particles. The tuning of the aforementioned properties will then allow for control over the expected reactions to stimuli. In the case presented, temperature change is used to trigger

the transition, but in the proposed research other stimuli including the absorption of specific molecules, or change in pH will be used.

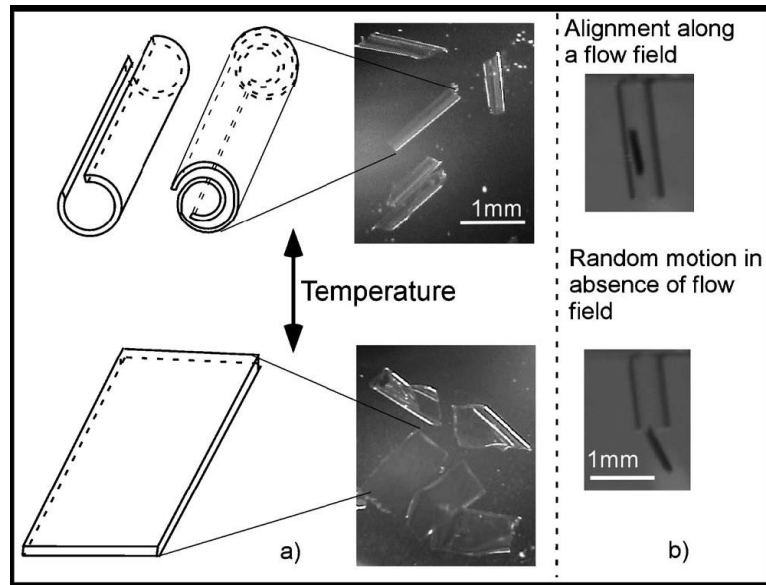


Figure 1-5:a) Shape transition triggered by temperature. b) Alignment of particles in forced flow, top; and random flow bottom [1]

The advantages of this technology are as follows:

1) Sensitivity: The dimensions of the particles and the residual stress built into the bi-layer's interface can cause shape transition to occur under a very small change in environmental conditions (for example temperature) providing sensitivity that can be tuned by geometry and material properties.

2) Speed: The dynamics of the shape transition depends on the heating/cooling rate used. For example, as reported in [1] the average unfolding rate of the PDMS/Au particles increases significantly with the temperature used to trigger their response, ranging from opened particles per minute of 0 to 0.42 and finally to 40.6 at T_{ambient} , $T=85\text{ }^{\circ}\text{C}$, and $T=124\text{ }^{\circ}\text{C}$, respectively. The transition time of a single particle is about 5-10 sec when the particles are triggered by heating at $110\text{ }^{\circ}\text{C}$. The dependence on the particle radius and lateral

dimensions of the flat bilayer on the transition speeds can be designed for different applications by altering geometric and material properties.

3) Magnitude of change: The shape transition results in changes of the flow characteristics and adsorption properties of the particles, which due to the nature of these transitions and the speed is very noticeable.

4) Versatility: Particles can be designed on several length scales, using a wide-variety of materials for a wide-range of applications.

5) Ease of manufacture: Processes simple to implement in a straightforward manner already exist for manufacturing of the responsive particles [1]

6) Ability to scale-up the manufacturing method.

If the elastomeric substrate is relatively thick, rather than bending and rolling of the planar heterostructure and the formation of 3-D structures, only the top thin metallic layer deforms, creating wrinkles as shown in Figure 1-6. The spacing and height of these wrinkles can be tuned by controlling the thickness and the modulus of the two materials forming the planar heterostructure.

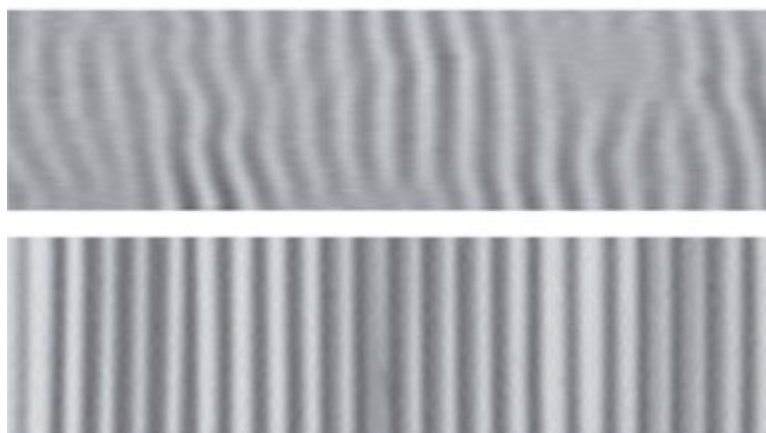


Figure 1-6: Wrinkles formed from pre stretching PDMS prior to Au deposition [42]

The expectation in working with thin bilayer structures is basic mechanical principles behind multilayer cantilever beam structures hold true. However, structures with thicknesses in the nano and micro scale could have thermo and mechanical properties that differ from bulk. Stress measurements in the thin film have been investigated with curvature measurements through the Stoney formula which was developed in 1909. The equation is given as[43]:

$$\sigma_f = \frac{E_s h_s^2 \kappa}{6 h_f (1 - \nu_s)}$$

The subscripts representing the film and substrate properties are s and f respectively. The h is the thickness of the layers, ν is the poisson ratio, E is the elastic modulus and κ is the curvature. The assumptions for the above equation are:

- The film and substrate have a uniform thickness with the substrate thickness much larger than the film thickness
- Strains and rotations of the system are infinitesimally small
- Film and substrate are homogenous, isotropic, and linearly elastic
- Film stress are in-plane isotropic and out of plane direct stress and shear stress disappear
- System curvature components are equibiaxial while the twist curvature vanishes
- Surviving stress and curvature components are spatially constant over the whole surface

Variations and adaptations to this formula have been utilized throughout the years to relax the stringent assumptions [44]. For substrates with a film grown on them, the strain due to lattice mismatch is governed by the compatibility condition and Newton's third law. These two equations combined can be used to indicate that there is a bending moment due to mismatch strain with strain in one layer would have an opposite sign in the other layer. A modification to the Stoney formula, giving the curvature κ is:

$$\kappa = (6\varepsilon_m/h_s)(h * E)[(1 + h)/(1 + h * E * (4 + 6h + 4h^2) + h^4E^2)]$$

where $h = \frac{h_f}{h_s}$ and $E = \frac{E_f}{E_s}$ [45].

The strain ε is the uniform mismatch strain in the film, defined by the processing history and the different coefficients of thermal expansion in the material. For example the residual strain in a PDMS-Au interface is due to the differences in the coefficient of thermal expansion of the two materials. This residual strain is a result of (i) PDMS film shrinkage during curing, (ii) PDMS film shrinkage due to cooling from the curing to ambient temperature and (iii) the internal stresses of the Au film during deposition as thin film processes can lead to films in tensions.

This relationship is valid for any material combination (arbitrary ratios of film thickness and modulus) given strong interfacial adhesion and can be used to design responsive structures. When the lateral dimensions, L and W , of the bilayer are much larger than its thickness and characteristic bending scale ($L_o=2\pi\rho$), i.e. $L \sim W \gg h_s+h_f$ and $L \sim W \geq 2\pi\rho$, then both folding directions are preferred equally and tubes (rolling along L) or rings (rolling along W) form. In the case that $L \geq W$ and $W \leq 2\pi\rho$, open structures such as coils or arcs form as shown in Figure 1-7.



Figure 1-7: Schematic of a strained bilayer film folding into a tube when W is large, but into a coil when W is small. The arrows indicate the folding direction[39]

1.2 Artificial Cilia

Smart materials have been used to fabricate structures of various shapes and sizes that mimic structures found in nature, such as Gecko foot [46] and lotus petals [47]. Another structure commonly found in nature, that is of interest in this research is cilia. Cilia is a cell organelle that is shaped like tiny hairs with a length of $\sim 20\mu\text{m}$ and high aspect ratio (length/diameter ratio).

Interfacial biological surfaces are often lined with tiny elastic cilia as seen in Figure 1-8. Cilia are categorized into two groups, motile and passive cilia, which are involved in different physiological processes including particle transport, mucus removal, feeding, propulsion, etc. [48-51]. Cilia through its movement can help actively modify the surroundings. For example, in the body, regulation of fluids in the lungs and kidneys are dependent on the cilia as seen with the organelles in Figure 1-8a. Cells that swim on the microscale use beating flagella and cilia for propulsion rather than structures closer to the propellers used by humans on boat. Marine organisms that rely on suspension or filter feeding employ various cilia for trapping food particles from streaming fluids [48].

Cilia arrays have been designed to affect the particle movement in fluids and much research has been done on the actual movement of cilia itself. Much of the research is focused on motile cilia as the active motion of cilia has been shown to be very efficient on the microscale. Research in this field is focused on harnessing cilia movement for pumping and mixing. A variety of artificial cilia have been created that react to magnetic fields, light, pH changes, and electrostatic forces. The idea is to create the hair-like geometry with smart materials to imitate the beating motion of natural cilia which is asymmetric.

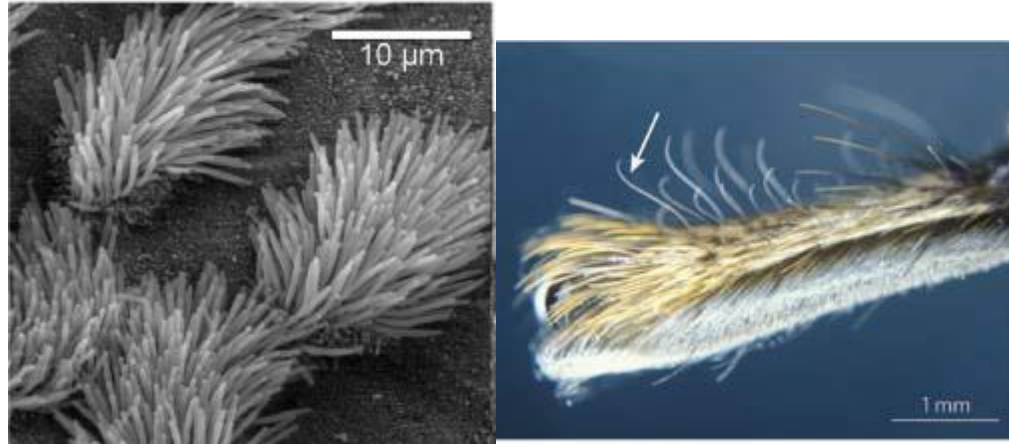


Figure 1-8(a) Lung cilia [52] (b) sensory cilia on a spider leg [53]

The fabrication techniques of artificial cilia in literature typically follow those outlined in the PDMS fabrication section. Photolithography was utilized to create rectangular shape magnetic cilia, as seen in Figure 1-9, uses a uv curable polymer with magnetic particles [54-57]. Soft lithography techniques were utilized previously to fabricate arrays of nanostructure columns [58] which were later actuated by surrounding the structures with hydrogel [6]. A multimixer fabricated from a laser cut mold functioned similarly to cilia multimixers [22], utilized a magnetic composite polymer. With some casting processes, the mold used is destroyed during structure release. Polystyrene sheets punctured with needles were used to create pillars that were released when the polystyrene was dissolved in chloroform. A porous membrane [4] formed through tracked etching rather than a custom mold allowed for the creation of nanocolumns. Track etch membranes have controllable fabrication through use of a charged ion beam that bombards the substrate and leaves a track. This track is then etched away preferentially so pores are tunable. This approach is limited by the cilia arrangement as the porous membrane has randomly distributed holes meaning each membrane produces a different pattern.

mold fabrication. However with the micron sized cilia, other shapes can be generated with the correct masking in photolithography; the most common shape however are rectangular due to the known geometric properties of cantilever beams. Similarly with the self-assembly, the shape is constrained by the particle size, which is on the order of microns, and by the shape the particles assemble themselves into.

Arrays of synthetic cilia as an active surface have been investigated as a way to direct fluid flow so particles can be directed towards or away from the surface. This is leading to the creation of self-cleaning surfaces as well as the possibility for particle guides to sensing areas and for filtering applications. Theoretical simulations of the fluid motions around cilia have revolved around motile and non-motile cilia. Simulations of motile cilia that are periodically arranged have been demonstrated by different groups. The important cilia parameters are the particle cilia adhesion, stiffness of the structure which is controlled by both dimension and modulus, and oscillation speed. [60-63]. Non-motile cilia were designed and it has been shown that tilted surface posts generate secondary flow fields that increase lift forces compare to the corresponding forces of smooth surfaces, with the maximum forces observed at a tilt of 40° [64]. It was also shown that the direction the cilia are placed in the flow, either against or along the flow, dictates whether particles will be moved towards or away from the surface respectively [61, 65] as shown in Figure 1-10. These theoretical studies have been the motivation of this research. The idea is to create self-cleaning surfaces decorated with periodic arrays of cilia that will repel particles away from the surface.

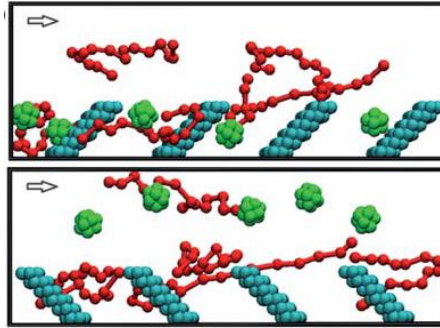


Figure 1-10: Simulation of cilia array for particle deposition and removal[61] , Cilia tilted along fluid flow (top) and against (bot)

1.3 Nanoporous (NP) Metal Foams

The laminated composites investigated in this research are made using PDMS substrate and nanoporous (NP) metal foams. NP metal foams are three dimensional structures made from connected metallic particles with a porosity of at least 50% in the form of submicron interconnected pores. The unique nanostructure allows for very high surface area, low density, and high strength to weight ratio while still maintaining some of the material property of the base metal [66]. Common fabrication techniques are sol-gel approaches, combustion synthesis, and templating.

The sol-gel combustion process starts off with a solution that forms a gel-like system comprised of metal nanoparticles and a polymer network. This network is then dried to create an aerogel and that aerogel is combusted to cause the necessary reaction to create the desired material network [67-70]. Various nanofoams were created with Co, Fe, Ni, Cu, and Ag. Material choice is a concern as the final step typically has a reduction of the metal oxide to the pure metal form. Materials that don't form stable oxide networks or reduce to the metal from the oxide in the combustion process might not be usable.

Combustion synthesis, also referred as self-propagating high temperature synthesis, relies on the energy released from the combustion of the precursor materials to initiate

reactions that have high activation energy barriers at room temperature. An important aspect to the correct structure formation is chemical composition of the pellets that are to be ignited. This technique with bistetrazolamin metal complexes was demonstrated for Co, Fe, FCC Cu, and Ag [71].

Templating is the approach of depositing metals on a template structure of the desired porosity and removing the template structure post deposition. Depending on the template, the foam structure can be either disordered or ordered. Template material have included beads formed from polystyrene [72] and colloidal silica. MNF with ordered structures was discussed in [73] which utilized block-copolymer supramolecules as the template material. In this study, the PS-b-P4VP created a network within the pentadecyl phenol (PDP) matrix. The PDP matrix was removed and the resulting structure had metal deposited on it prior to pyrolysis.

A variation on templating is dealloying which uses an alloy of a base material along with other reactive metals. The base material must be in sufficient enough concentration to form a network within the alloy. The reactive metals are etched away, either through acid or electrochemical processing, leaving the base material in its network. Dealloying limitations are the alloys that can be used and the size restrictions due to diffusion limited processes. However, the fabrication method of choice is dealloying for this thesis to avoid the high temperature needed for the pyrolysis or combustion processes needed in some of the sol-gel, templating, and combustion synthesis processes.

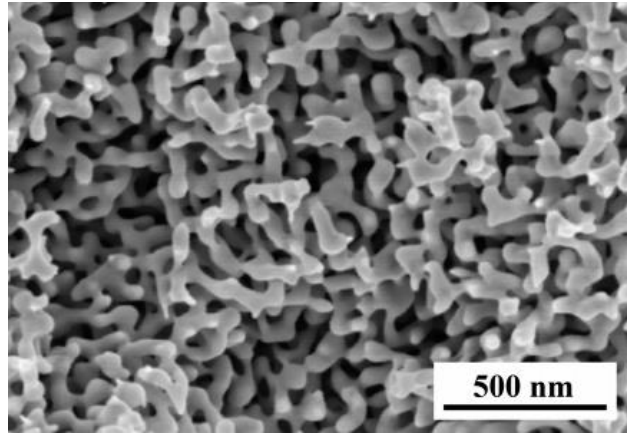


Figure 1-11: SEM micrograph of nanoporous Au [74]

The material properties of metal nanofoams have been shown to depend on the geometry of the foam itself [74]. This was shown with nanoporous Au, shown in Figure 1-11, where the gold gained strength with decreasing length scale of the pores and ligaments, with the expectation that at around 10nm, the strength should start to decrease rather than increase. Further research [75] has shown that unlike traditional low density foams, whose ratio of foam modulus to strut modulus are known to scale to $(t/l)^4$, where t and l are the strut thickness and length respectively, NP metal foam follow a modified scaling. The modulus of the struts deviates from bulk when the size of the internal scale or the size of the strut is smaller than 10 nm.

The use of nanofoams as part of a planar heterostructure is a novel application of the standard bilayer approach. It is necessary to utilize a substrate to mount the nanofoam due to the fragility of the foam structure itself. With the addition of applied compressive stress, the nanofoam structure should become denser as the foam is forced together and thus the bilayer properties can be tuned. Strain engineering has been employed to create responsive 3-D structures using metal/PDMS bilayers[1], however, there are no studies on using NP metal foam layers on elastomeric substrates. The resulted responsive structures

are expected to be multifunctional and exhibit a wide range of properties that will be significant different in the two states (triggered vs non-triggered).

1.4 Thesis Goal and Objectives

The goal is to understand the role of elastomers, PDMS, on the responsive behavior of smart materials. The two specific objectives are:

- Design and fabricate and characterize a biomimetic microstructure that undergoes magnetic actuation using a filler reinforced PDMS composite
- Develop a smart material with laminated structure utilizing strain engineering

The design of the first elastomeric composite is based upon cilia, a microstructure found on many cells whose primary purpose is to provide movement on the microscale. These hair-like structures are used for filtration in the lungs so the intent is to create artificial arrays of elastomeric material that could then be potentially used for self-cleaning or filtering. The actuation of choice is magnetism as the inspiration for the specific design came from an application that involves a fluid environment, where electrical actuation is not feasible. To facilitate moving magnetic microcolumns, iron contained PDMS composites will be molded and characterized so that filler concentration can be optimized with relation to modulus to allow for better moving structures.

The second objective utilizes the elastomer as a substrate to a porous metal thin film layer to create a planar heterostructure. In bi-layer systems, the differences in material properties between the two attached layers results in residual stresses. The structure can then be actuated through temperature or solvents due to the change in a single material. As

the porous thin film is fragile the elastomeric film can provide an adequate backbone while still maintaining its elastic features.

Chapter 2. PDMS Composite Cilia Arrays

Cilia are an important cell organelle that allows for movement for certain cells and filtration within the body. Biomimetic artificial cilia have previously been fabricated as a way to create pumps and mixers at the microscale. There has been simulation of cilia arrays that demonstrate the particle separation in flow due to passive cilia arrangement. The intent is to construct elastomeric cilia arrays that could be used for that purpose.

The chapter will discuss the design concept, the structure and properties of the artificial cilia including dimensions and size, material selection, limitations and potential of fabrication methods and response of the arrays to magnetic field. The fabricated structures are characterized optically to confirm physical dimensions and dispersion and distribution of iron based filler particles within the elastomeric matrix. The modulus of the composites is determined as a function of the magnetic particle content using dynamic mechanical analysis. Finally, the cilia decorated structures are actuated by an external magnet and their response i.e., bending angle, is characterized as a function of the magnetic filler content.

2.1 Design

Considering that many parameters, controlled experimentally, have counteracting effects on the response of the surfaces decorated with cilia arrays, the first step is to identify the most dominant ones. For example, the modulus of the cilia, which can be controlled by either tuning the monomer to curing agent ratio of elastomer, or the magnetic particle content, affects the stiffness of the composite cilia and thus their response. In addition to parameters related to the material composition, geometric parameters such as the aspect ratio (height to diameter) of the cilia also affects the stiffness of the cilia arrays.

For the following analysis, the cilia are considered as ideal circular cantilever beams and the force applied by the external magnet is considered equally distributed along the beam/cilia length. In such a case the maximum deflection is given as:

$$\delta = \frac{\omega * L^4}{8 * E * I} \quad (1)$$

with I defined as

$$I = \frac{\pi * r^4}{4} \quad (2)$$

where ω , L , E and r are the ratio of total force per length, the length of the cilia, the modulus and the radius of the cilia respectively. Solving for stiffness one gets:

$$k = \frac{8EI}{L^3} = 2 * E * r * \left(\frac{r}{l}\right)^3 \quad (3)$$

According to Eq. (3), it is obvious that the aspect ratio of the beam/cilia has a much stronger effect on the stiffness than the modulus.

Specifically, for magnetic composite cilia, Evans developed an analytic continuous model [52] that estimates the total energy of a single cilia with the assumption that the magnetization magnitude is only dependent on the internal field and not on orientation. Of note, their material was a nanosized maghemite particle. The energy can be written as:

$$u = \frac{1}{2} EI \int_0^l \frac{1}{R(s)^2} ds - \frac{1}{2} \mu M^2 f^2 V (N_x - N_y) \cos \theta^2 \quad (4)$$

where θ is the angle difference between the field and bend angle, f is the volume fraction of the magnetic particles, μ is the magnetic permeability, M is the magnetization per unit volume of the material, R is the radius of curvature of the cilia as a function of s , which is the distance along the cilia from the base, N_x and N_y are the demagnetization factors that are parallel and perpendicular to the cilia axis respectively. An assumption is that the

magnetization of the polymer composite is linear with respect to the volume fraction and that the magnetic moment is equal to $M \cdot \text{volume of the structure} \cdot \text{volume fraction}$.

The torque is then calculated by taking the derivative of the energy. An assumption is that the magnetization is linearly correlated to the magnetic filler's volume fraction. This equation is also simplified with the assumption that the radius of curvature is constant, the magnetic force is equal to the magnetization multiplied by the volume fraction, and for high aspect ratios that $N_x - N_y = .5$. The condition set for high aspect ratio is greater than 20; with an aspect ratio around .1 the difference is around .44. With the assumption of constant curvature radius, the radius is then given as $L/(2 \cdot \psi)$, where ψ is the bend angle. After all the assumptions, the torque is given as:

$$\tau = \frac{\pi E r^4}{L} \psi - \mu M^2 f^2 V (N_x - N_y) \cos \theta \sin \theta \quad (5)$$

The maximum force occurs at $\theta = 45$ and if $N_x - N_y = .5$, then the bend angle due to magnetic field actuation would equal:

$$\psi = \frac{\mu M^2 f^2}{E} \left(\frac{L}{2r}\right)^2 \quad (6)$$

Again, based on the above analysis, it is clear that the aspect ratio affects the stiffness of the beam more than the elastic modulus does. A beam with a larger aspect ratio, with higher or smaller diameter, would allow for less required force in order to bend/deflect. The elastic modulus can also be tuned but the physical dimensions have more of an impact on the forces required to bend the structure. With the goal of controlling the bending and getting the most response of the structure using the minimum possible force a high aspect ratio of about 10 is chosen. Although the higher the aspect ratio the lower the force required for actuation, the fabrication methods set the upper limit to the aspect ratio of the cilia that can be made.

The purpose for fabricating the magnetic cilia is for its eventual use in fluid environments where the cilia will help either trap to or repel from a surface particles dispersed in solution depending on whether the cilia are tilted against or parallel to the flow field. As an approximation, it is assumed as before the fluid is acting on a uniform circular column and creates a constant distributed load. Based on mechanics of cantilever beams, the distributed force required for a specific angle bend is given as

$$F = \frac{\pi}{8} * E * (d/l)^4 * \Delta \quad (7)$$

where the angle would be found to be Δ/l with D and l being the diameter of the cilia and length of the column respectively. As the flow would potentially be actuating the structure, the assumption is that the drag force from the fluid flow is the only force causing the beam to bend. This drag force is found to be

$$F_d = C_d * \frac{1}{2} * u^2 * A \quad (8)$$

where C_d and u are the drag coefficient and fluid velocity respectively. As a starting point, the drag coefficient is given as $13.6/Re$ with the assumption of a circular disk parallel to flow at Reynolds number lower than one, where Re is the Reynolds number and is given as $\frac{\rho * u * d}{\mu}$. ρ , μ are the density and viscosity of the fluid and d the diameter of the circular disk. From this, the expected load to bend the beam and subsequently the necessary fluid velocity can be calculated. The table below shows the load required to bend the cilia a specific angle and the corresponding velocity of the fluid. Cilia with an aspect ratio of seven which is the approximate aspect ratio of the fabricated cilia is considered.

Table 1: Average fluid velocity based on bend angle, columnar aspect ratio of 7, elastic modulus of 1 MPa

Angle (°)	Load required (N)	Velocity (m/s)
5	6.98E-08	1.47E-01
10	1.39E-07	2.92E-01
15	2.07E-07	4.36E-01
20	2.74E-07	5.76E-01
25	3.39E-07	7.12E-01
30	4.01E-07	8.42E-01
35	4.60E-07	9.66E-01
40	5.15E-07	1.08E+00
45	5.67E-07	1.19E+00

The low Reynolds regime fits the fluid that actual cilia would be moving in. Note that the drag coefficient decreases as a function of increasing Reynolds number with the drag coefficient dropping from around 10 at Reynolds number of 1 to approximately one at Reynolds number of 1000. As the drag coefficient decreases, the drag force becomes lower, indicating that it would take even faster moving flow in order to bend the pillars. As the force is proportional to velocity squared, the increase of modulus of the cilia due to the addition of the magnetic iron particles will increase the velocity necessary to bend the structures. Just as a reference it is noted is that the velocities for angles larger than 20° indicated in the table are higher than the flow of blood in the body [76].

The same properties that influence the bending of the cilia due to magnetic force are also prominent in determining the fluid velocity necessary to bend the cilia. The main concern is still the aspect ratio of the cilia as the fluid velocity scales to the square root of the elastic modulus versus scaling to the square of the aspect ratio. Structures that are going to be actuated against the flow will also need to overcome the fluid force so a balance must be struck. In practice, the application will determine whether it is more useful for the structure to bend in the fluid flow or to stay straight.

2.2 Materials selection

The material chosen to be the elastomer matrix for the composite is PDMS, specifically Sylgard 184 from Dow Corning. The polymer is a two-part mixture, with a thick elastomer base and a cross linker. The ratio typically used in literature and recommended by the manufacturer is a 10:1 ratio of base to crosslinker. This ratio can be modified to tune the final elastic modulus of the material, with increasing ratios leading to decreasing elastic modulus. Similarly, increasing curing temperatures are correlated with increasing elastic modulus. The curing time of 24 hrs at room temperature would result in the most flexible material, however the time spent outweighs the benefits of the long cure time. A shorter cure time with a higher temperature was selected, specifically 80 °C for 1 hr.

As a responsive structure is desired, magnetic actuation is the chosen method because it does not need physical connections to actuate and can be utilized in environments that methods such as electrostatic actuation cannot be used. The magnetic filler of choice is iron because as a ferromagnetic material it can experience more force from a magnet. The iron particles, specifically Carbonyl Iron, were purchased from Sigma Aldrich. The particle size is between 6 and 9 um with a purity of >99.5%. The choice of a ferromagnetic material stemmed from the need for a high magnetic response. The high iron purity and large size leads to the assumption that bulk material properties of iron are applicable for these structures.

2.3 Fabrication Method

Microcasting/micromolding is the chosen method to fabricate the soft cilia arrays. The process preferred as it is repeatable and requires less specialized equipment/processing

to create the arrays. The fabrication process consists of two steps, the first one is the fabrication of the mold and the second one is the casting of the iron particle/PDMS solution into the mold. Various approaches to make the mold were followed in this research depending on the geometric characteristics (diameter, height and spacing) of the cilia. For cilia with diameters smaller than 20 microns, soft lithography can be used whereas for cilia with larger diameters conventional material removal processes such as laser cutting are employed.

2.3.1 Mold fabrication

Su8 photoresist was used to make a mold through conventional photolithography techniques. The photoresist was specifically designed to provide features with aspect ratio of ~10:1. As the su8 a negative photoresist, the mask used was a transparency with an array of black dots. The su-8 was spun on 4" wafers to smooth out the su8 layer. The mask, a printed transparency was used with a UV filter in the exposure process. The exposed wafers were then developed in a sonic bath to aid the developer to get to the bottom of the hole. The intent was to spin a 100 um thick su8 layer and utilize a 10 um holes. The final result was a mold whose holes were 10 um in diameter but the depth of the hole did not reach through the silicon substrate so the holes and consequently the molded cilia had a small aspect ratio. The geometric features of the mold are shown in Figure 2-1.

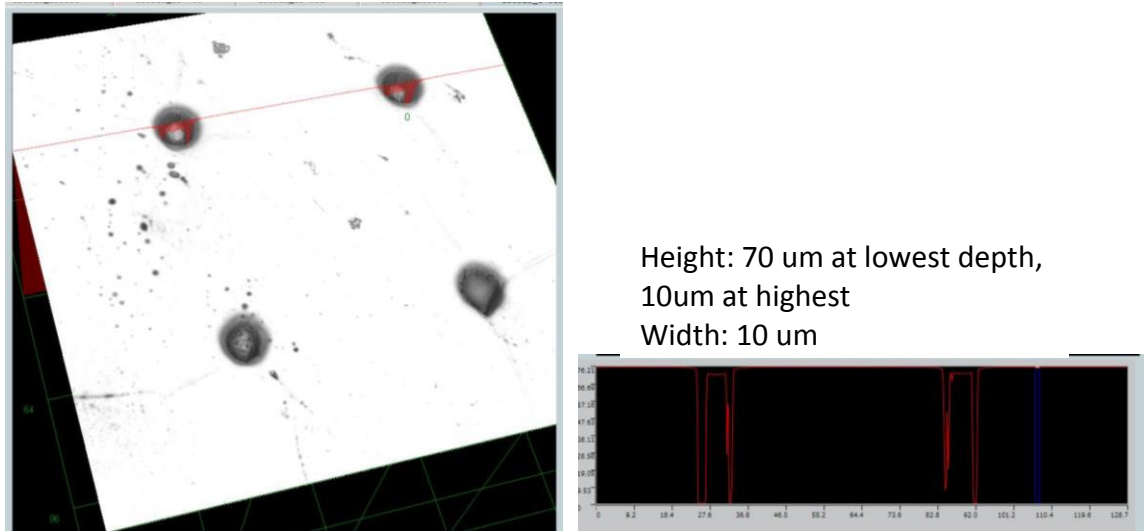


Figure 2-1: (a) Laser confocal image of su8 mold, (b) Height profile of cross section

The issue with the su8 fabrication process is attributed to the high areas of the su8 that are crosslinked. There is a concern that the light propagates internally which could potentially crosslink the polymer at the bottoms of the holes, leading to partially filled holes. A better method could be using the negative of the dotted mask which would create su8 pillars rather than holes. These pillars would then be used to fabricate the mold, shown in [36]. The reasoning is that even if there is light leakage, the pillars would be separated far enough that they wouldn't interfere with each other.

The mold fabrication method chosen was laser cutting using acrylic. Laser cutting is a fast process, even though it is serial in nature. A disadvantage to using laser drilling is the non-uniformity of the fabricated hole. Using a single beam, a round hole will eventually widen at the top due to the localized heating. This resulted in the hole being conical in shape, with a larger diameter at the top. Acrylic was chosen as a the mold material in order to keep the fabrication simple and due to known processing conditions, and rigidity required when working with materials on the millimeter scale. Thin films of both metals and polymers, like Kapton, could be utilized with the laser machining. However, metal,

even those a few millimeters in thickness, requires much more energy to cut through than plastic and in most cases would require machining rather than laser cutting.

The molds were arrays of thru holes placed in a rectangular pattern. Arrays were fabricated with 3 mm spacing between the holes with the hole diameter tuned to the smallest size the laser could output. The holes were fabricated as thru holes to ensure that the structures were all the same length. The duration of the laser pulse can be calibrated to determine hole depth. However, thru holes eliminates the possibility that the fabricated holes are not all the same depth due to variations in the laser fabrication process. The acrylic thickness was chosen to be 3mm, based on the 300 um diameter of the fabricated holes. The acrylic was purchased as a sheet, which was manufactured with standard thicknesses, from McMaster Carr. Due to the nature of laser fabrication, it is possible to fabricate holes that are not just circular in shape. However, these shapes are limited by the resolution that the laser cutter can provide.

The laser cutter utilized was a Trotec Speedy 300. With this machine, the average top size is around 500um and the exit hole is approximately 300um. As such, the top surface was kept as the side that would be exposed and where the liquid pdms solution would be introduced. Figure 2-2 is an optical micrograph of the acrylic mold.

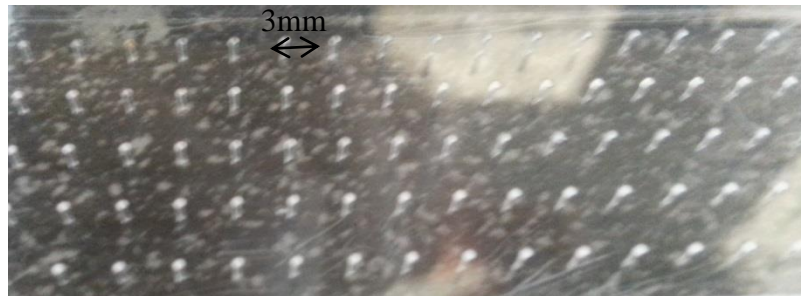


Figure 2-2: Laser cut acrylic mold

Alternative methods and materials to the acrylic mold fabrication were tried including laser fabrication with a Kapton film, Shrinky-dink as the mold substrate, wax as the mold substrate and su 8 mold. The first three processes mentioned relied on destructive processes to fabricate the mold. The su8 fabrication relied on standard photolithography techniques as discussed above.

The usage of kapton film allowed for smaller structures as the kapton film itself was close to 75um in thickness. In order to get the high aspect ratio, the holes that were fabricated were around 10um. However, the same issues with using the acrylic are apparent when looking at pillars fabricated from the mold. This makes the anticipated aspect ratio smaller than desired as even a small change of 1 or 2 um in the mold hole diameter due to the heating results in huge changes in the aspect ratio when working on such a small scale. Using acrylic was a feasible alternative to this material, as the acrylic thickness is not a limitation and thicker acrylic sheets could be used to allow for cilia with larger diameters while still maintaining the desired high aspect ratio. An optical micrograph of the cilia array made using the Kapton mold is shown in Figure 2-3. As shown, the cilia are more of a conical shape and of low aspect ratio.

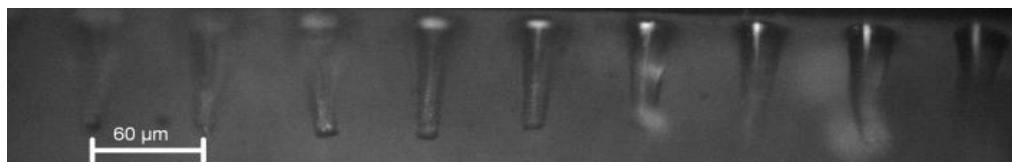


Figure 2-3: PDMS pillars made from laser cut Kapton mold

Polystyrene in sheet form was also investigated as a potential mold material, reported also elsewhere [27]. The polystyrene sheets shrink to approximately $\frac{1}{2}$ the width and double the thickness. 33gauge needles were used to puncture the holes into the sheets, resulting in a .26mm hole that would shrink to around .13mm. The PDMS however was

not easily removed from the polystyrene mold. The usage of a solvent to dissolve the mold to release the cilia structure made this process infeasible due to the mold being single use as well as the fact that the solvent would also swell the PDMS.

Similarly the concept of using needles to fabricate the mold out of soft material was explored. The needles were arranged in an array and used to puncture wax. The intent was wax molds could be melted to release the polymer structures and the needle array could be repeatedly used to puncture the soft material. The issue with wax molds was the wax residue left on the structures and the limited temperature range useable to cure the polymer as elevated temperature would soften and deform the mold.

2.3.2 Casting

To fabricate the structures, the liquid polymer is mixed with the magnetic particles and poured into the mold followed by curing. Specifically, the liquid monomer and magnetic particles were measured by weight and manually mixed together for 5 minutes. The crosslinker was then measured and added into the monomer-particle solution. As stated earlier, the weight ratio of the monomer to crosslinker used was 10:1. This final solution was then mixed manually for 5 minutes and degassed in a vacuum environment for a minimum of 30 minutes to ensure there was no air trapped in the final solution before curing occurs. The iron content in the composites was approximately 20, 30, and 40% by weight.

The mold itself is placed with the smaller holes face down on another sheet of acrylic so that the hole bottoms are sealed off and the structures can be removed post cure. The final iron/PDMS solution is then poured into the mold. The molds are degassed for five minutes to remove air bubbles that may have been introduced to the PDMS during the

pouring of the solution as well as any air that may have been trapped at the hole bottom. The mold is then placed into the preheated oven at 80°C and baked for 1 hour.

To remove the cilia structures, the mold is first separated from the bottom acrylic sheet. In many cases, a small film of PDMS is formed on the back side which is removed by cutting with an exacto knife. The whole mold is cooled in a refrigerator for 30 minutes. This is meant to shrink the PDMS composite more than the mold which would allow for easier removal. The structures are then peeled out of the mold row by row.

The fabrication process of the surfaces decorated with cilia arrays is shown in details in Figure 2-4. The geometric features of the cilia including their diameter, height and spacing are shown in the optical micrograph of the iron/PDMS structure presented in Figure 2-5.

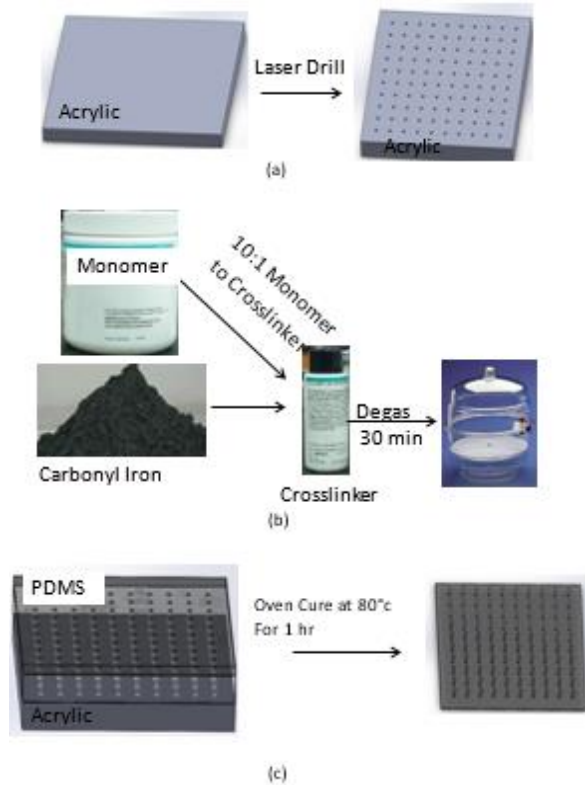


Figure 2-4: Fabrication process for the PDMS column structure (a) Acrylic mold fabrication, (b) PDMS/Fe mixture, (c) Pillar Array fabrication

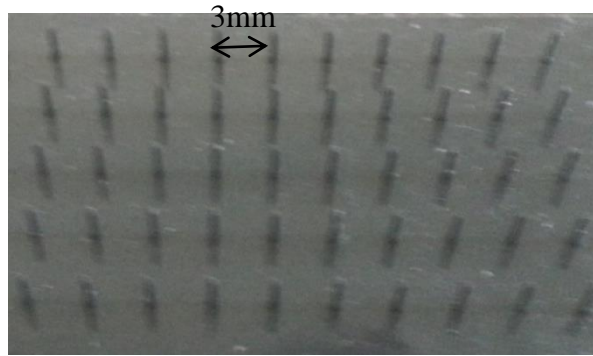


Figure 2-5: Released 40wt% Fe-PDMS pillars

2.4 Characterization of cilia arrays

The structures were characterized to determine both physical characteristics and the material properties. They were inspected visually under a microscope to confirm the structure dimensions. Similarly the dispersion was observed through SEM imaging and image analysis. The modulus was measured through stress strain curves obtained from dynamic mechanical analysis.

2.4.1 Shape and geometry

A microscope was used in conjunction with the Leica Application suite to measure the feature sizes at 10x magnification. As expected, the mold has holes of conical shape. The expected larger diameter was around 500um and the expected smaller one was close to 300um in average. This can be seen in Figure 2-6 with the top surface being very close to circular in shape. The shape of the hole bottom is not as circular. This is thought to be due to the inaccuracies of the laser cutter and possibility that the material deformed during cutting. The custom conditions of the laser cutter were chosen to minimize the energy required to cut the hole, as a full power cut would cause the hole to be too large. However, by minimizing the energy, it is possible that the cut is not as clean and the edges not as sharp.

The mold structure dimensions are born out in measurements of the actual pillar structures. The cilia have a length around 3mm, the thickness of the acrylic plate, as shown in Figure 2-7. The discrepancies in height are possibly due to the thin film of PDMS that forms between the mold and the holder substrate. The diameters were around 350 μm at the top of the structure and expanded to 450 μm at the base.

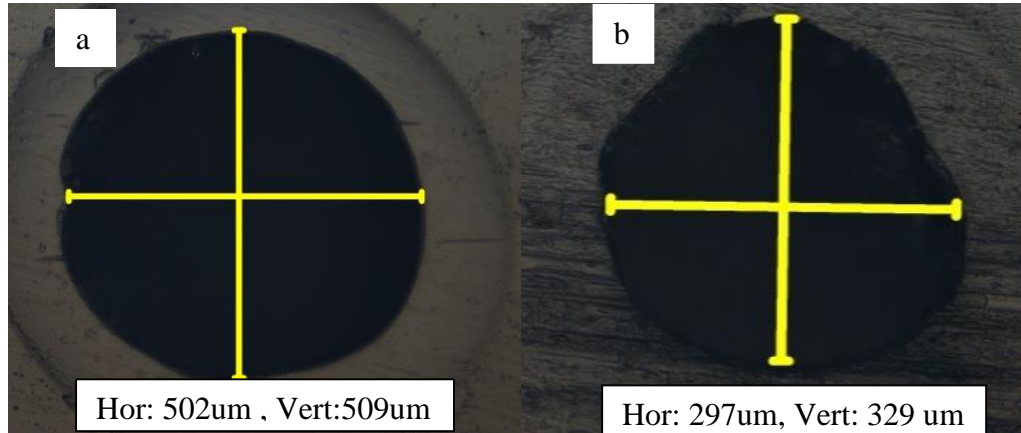


Figure 2-6: Representative images of (a) top and (b) bottom surfaces of the laser cut acrylic mold

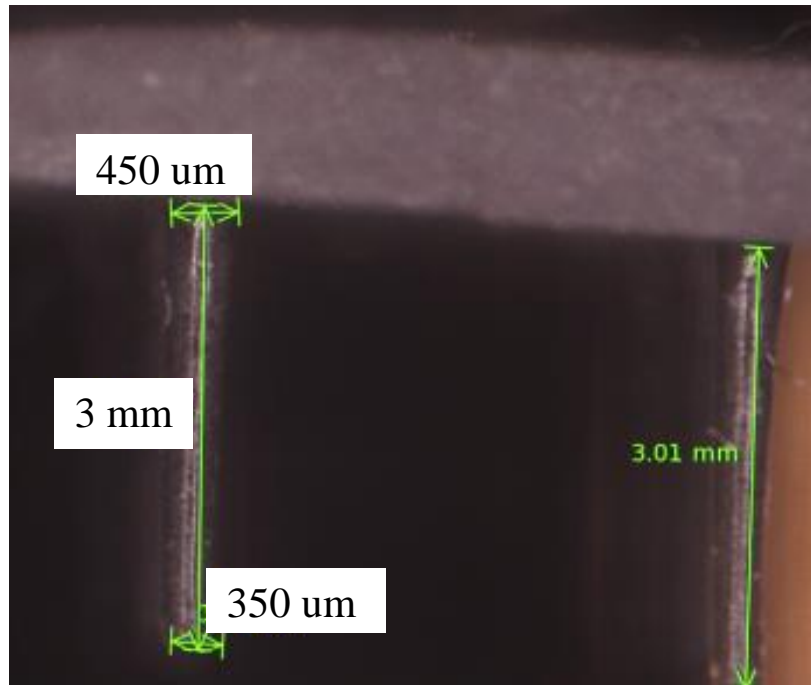


Figure 2-7: Representative image of polymer columns

2.4.2 Dispersion and Distribution of Fe-particles within the PDMS matrix

A Phenom Pro SEM was utilized to image the structures along and across the cilia axis. Both the circular cross section and lengthwise cross section were imaged to determine if there was a difference in the distribution and dispersion due to geometric constraints. The cross-sections were prepared by placing the structures in a freezer for at least 4 hours. They were then taken out and cut with an exacto knife. For the circular cross sections, the section was cut at least 1mm from the cilia tip. The cilia were cut in half along the length of the pillar.

The dispersion was characterized by measuring the size of the iron particle agglomerations using Image J software. The scale of the Image J program was set using the scale bar from the SEM image. Lines were drawn across the long side of the iron structures and measured. Representative images of the cross sections, both the circular and lengthwise cuts, are shown in Figure 2-8.

These measurements were tallied up and normalized by dividing the counts with the total number of structures to create a histogram that represented the dispersion. A total of eight images were used for each count. The bins were set at <5um, 5-10um, 10-15um, and >15um. The histograms comparing the differences between the circular and the lengthwise cross section were similar in distribution. As such, the dispersion is not directionally dependent so the charts shown in Figure 2-9 through Figure 2-11 are a combination of both the lengthwise and cross sectional distributions.

The dispersion, as noted previously, is important as the expectation is that the structure is homogenous. Significant agglomeration of the iron particles and inhomogeneous morphology would indicate that there is more force exhibited in the agglomerates than in the rest of the material so the assumption that the load is distributed would not be valid. Local agglomeration is expected with higher iron concentration. The concern is whether the agglomeration is prevalent enough that the material exhibits anisotropic behavior.

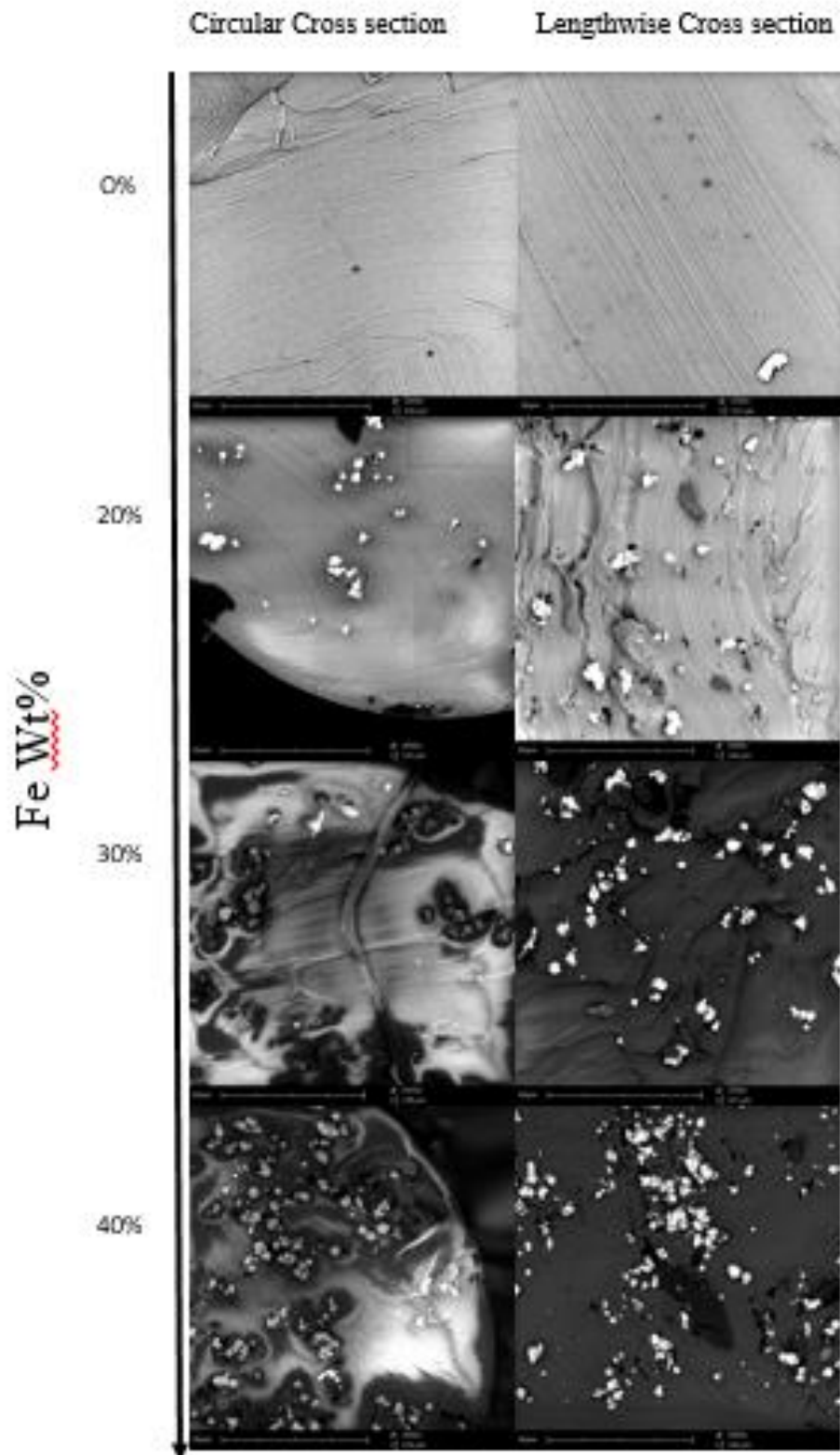


Figure 2-8: Representative cross section of PDMS/FE composite

There is increased localized agglomeration with increasing particle concentration. This is seen with larger agglomerates in the 5-10um and 10-15um ranges when the content of iron is increased to weight % of 30 and 40%. This is expected as the cross sectional area being investigated does not change while the amount of iron in the material is increased. However, the dispersion seems to be randomly distributed as the aggregates are spread out in their size. However, as the percentage of aggregates with sizes greater than 15um is smaller, the iron particles are not all concentrated together and the material can effectively be considered an isotropic material.

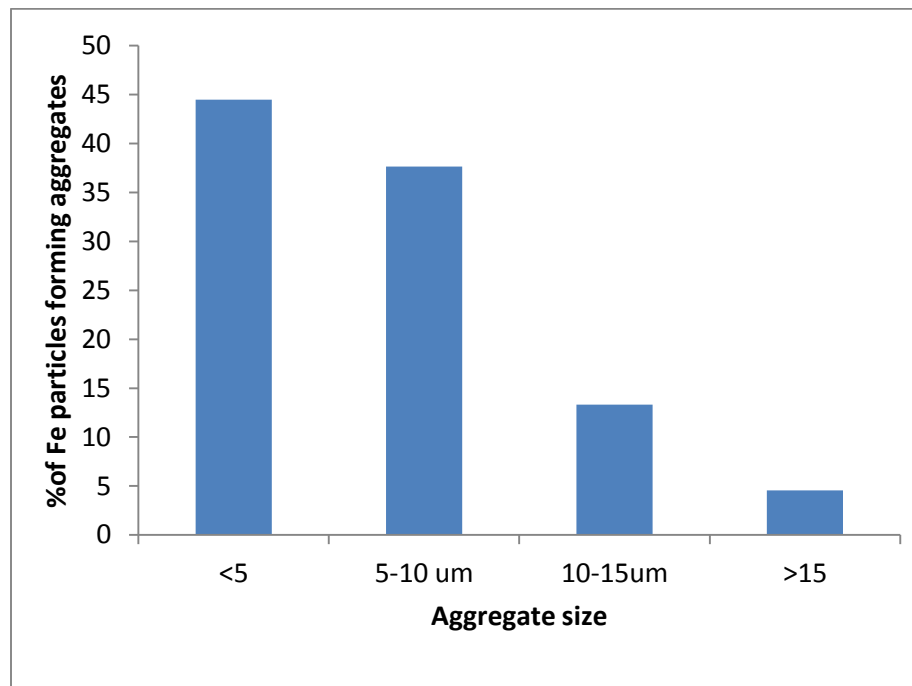


Figure 2-9: Particle aggregate size distribution for 20Wt % Fe

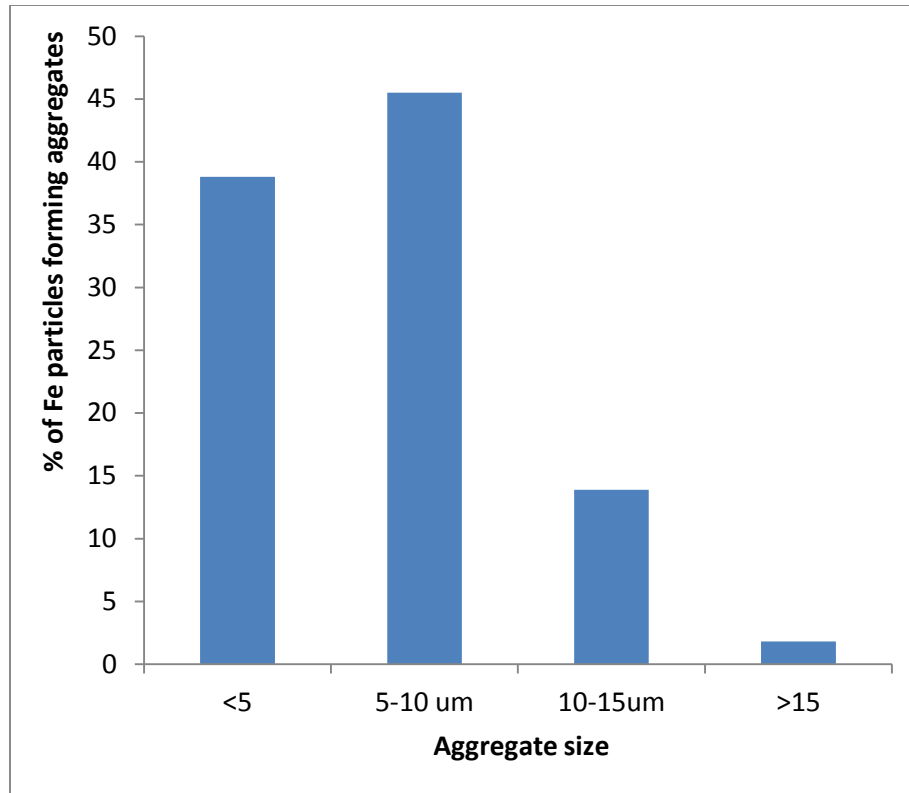


Figure 2-10: Particle aggregate size distribution for 30Wt % Fe

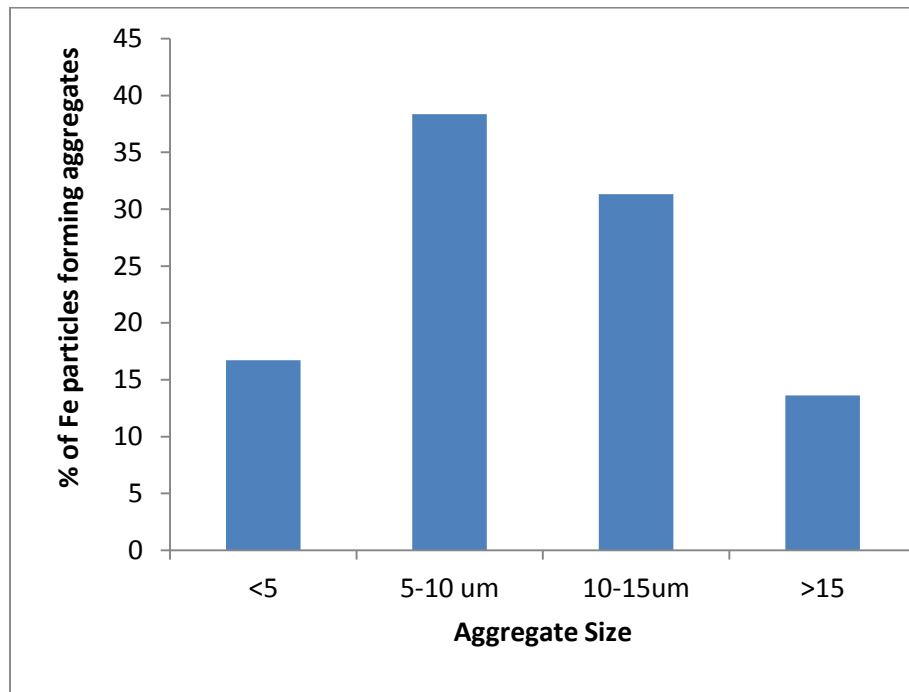


Figure 2-11: Particle aggregate size distribution for 40Wt % Fe

2.4.3 Modulus Measurement

The expectation with the addition of the magnetic fillers is that the elastic modulus will increase. The modulus was measured through the use of a TA Instruments dynamic mechanical analyzer. A uniaxial tensile force was applied to individual cilia that were cut out from an array and glued using Loctite onto custom-made 2 mm spacing paper tabs. The length of the cilia was measured prior to the attachment and set as the specimen length. The diameters on both ends of the cilia were measured using the Leica microscope and the average was used as input in the DMA. The modulus was determined as the slope of the stress and strain curve.

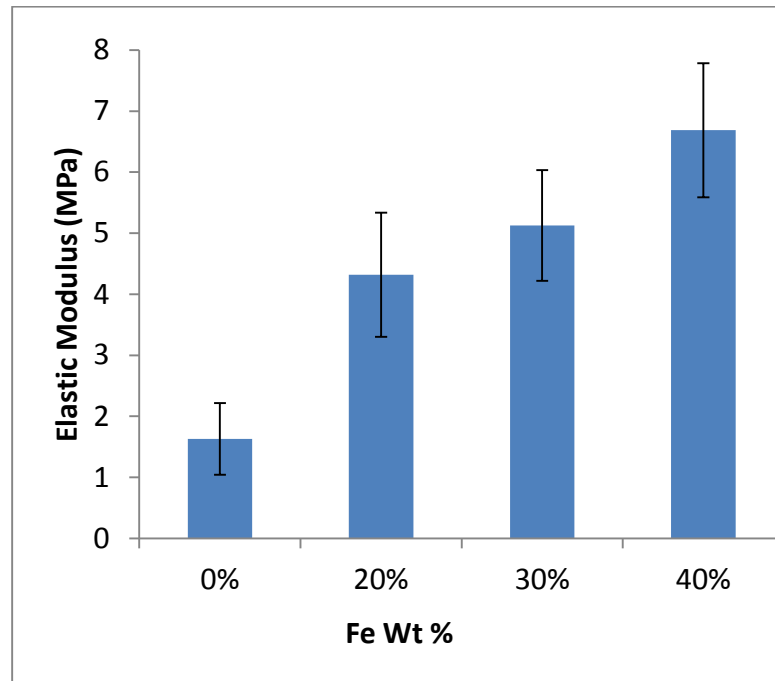


Figure 2-12: DMA measured elastic modulus

The modulus, presented in Figure 2-12, shows that increasing iron concentration stiffens the material. This follows expectation of strengthening of material when hard particulates are added to the polymer matrix.

2.5 Magnetic actuation of cilia arrays

The cilia arrays were actuated through use of neodymium magnets, purchased from K&J magnets. The magnet was taped down to a flat surface and the structures were placed 2.1mm away from the magnet. Images were taken and the angle of the tip was measured through image J. The bend angles measured were 20°, 40°, and 57° for the cilia arrays containing 20%, 30%, and 40% wt% of iron particles respectively.

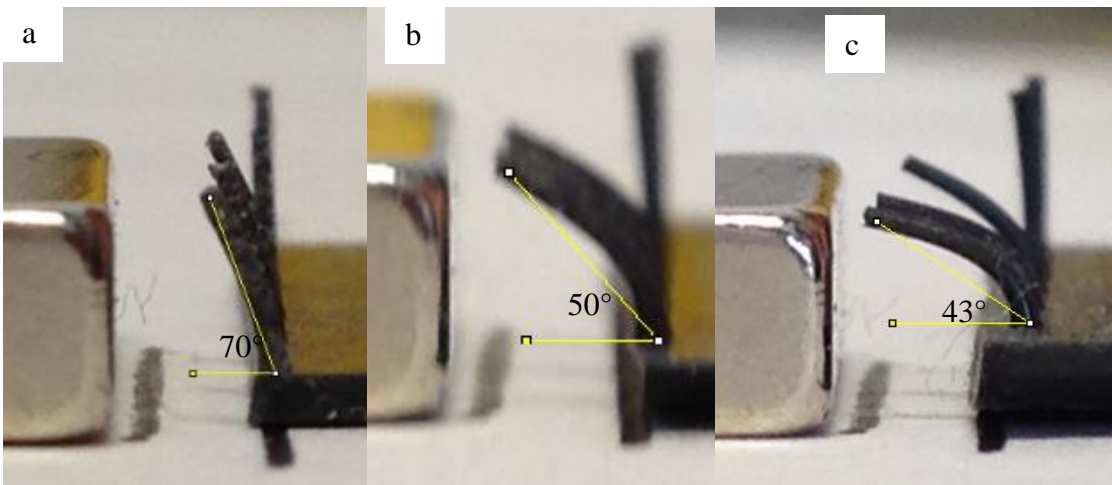


Figure 2-13: Neodymium magnetically actuated pillars: (a) 20Wt%, (b) 30Wt%, and (c) 40Wt% concentration

Using the previous stated assumption of a cantilever beam undergoing a distributed load, the bending angle is found to be $\theta = \frac{\omega * L^3}{6 * E * I}$. As such, the expected distributed load is $w = \frac{\theta * 6 * E * I}{L^3}$. As expected, with a higher iron particle content, there is a larger force which is reflected in the increased bend angles. By utilizing metallic filler, polymer composites can be fabricated to mimic hair like arrays with magnetic actuation. The actuation of the magnetic cilia has shown that a higher volume fraction of particles will allow for larger deformation of the pillars. However, there is an upper limit in the filler content as higher

filler concentrations will increase the elastic modulus so much that cilia may not be flexible enough to bend even in presence of stronger magnets.

2.6 Alternative approach to create tilted cilia

The concern with magnetic actuation is that the field strength from a single magnet is proportional to the inverse of the distance squared. This means that a single magnet that can move a single row of pillars will have difficulty moving another row. The magnetic actuation of multiple rows necessitates a uniform field. To move all the pillars together with a single force can be accomplished if the pillars are actuated by a surface attached to them. In order to do this, a thin PDMS film was attached to the top of the cilia. The fabrication process is shown in Figure 2-14. Two variations of this method were employed to fabricate this sandwich structure, with the top surface either being cured or uncured prior to attachment to the cilia.

In order to attach the cilia, it is necessary to separate the bottom substrate from the thin film. This was done with the same acrylic that the molds were made of as that is the minimum distance necessary between the two surfaces. To compensate for the film thickness, tape can be added to the acrylic stoppers. A thin layer of PDMS is spread on the thin film prior to curing so there is a glue to attach the cilia to the film. When using the fully uncured thin film, the cilia are placed into the liquid film prior to curing.

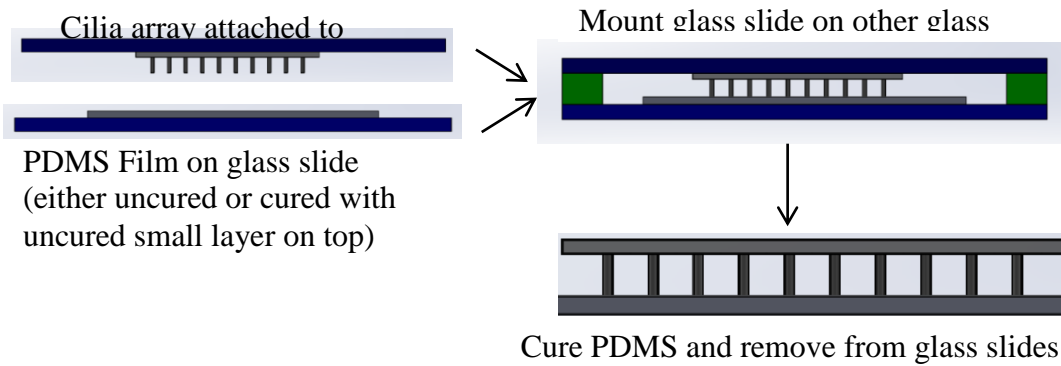


Figure 2-14: Fabrication process for sandwich structures

Fabricating the structures using the uncured film is expected to result in a stronger bond as the cilia becomes part of the whole film structure. The already cured film for a top layer process results in only a small external area as the bond. Empirically this was shown as structures made this way could sometimes be pulled apart and seen to break at the tip.

Fabrication in the above manner can result in a structure that does not bend as if they are cantilevers as seen in the larger bend angles in Figure 2-15. This is due to the fixed boundary condition that the attached surface imposes. For small angles, this is not as visible of an effect. For large deformations, the structure becomes a symmetrical shape that curves back. This is due to the connection between the film and the pillar trying to remain in an upright direction.

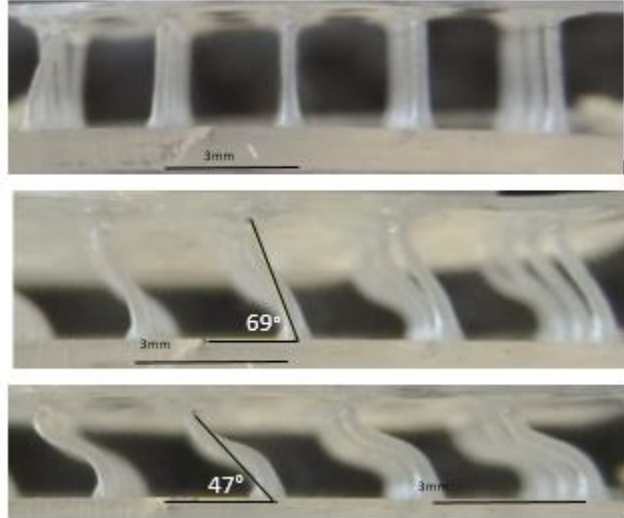


Figure 2-15: Sandwich Structure

2.7 Conclusions

The structure and properties of the artificial cilia including dimensions and size, material selection, limitations and potential of fabrication methods and response of the arrays to magnetic field were evaluated. Surfaces containing cilia arrays were made by magnetic composite formed from an elastomer and iron particles. The fabricated structures were characterized optically to confirm physical dimensions and dispersion and distribution of iron based filler particles within the elastomeric matrix. With standard mixing techniques, distribution were shown to be random but with agglomeration. The dispersion is relatively homogenous as the aggregate size distribution is predominately the individual fillers and small clusters. With higher concentration of iron filler, the aggregation is shown to be greater as there is larger number of large clusters. The modulus of the composites were determined as a function of the magnetic particle content with the expected result of increasing modulus due to addition of stiff fillers. The fabricated magnetic posts were actuated and it is shown that increasing weight percentage of iron filler results in a larger bend angle. However, it is expected that there is a limit to this effect

as the design evaluation has shown that higher modulus would result in less bending which the iron particles do contribute to.

Chapter 3. Laminated composites with PDMS and Nanoporous (NP) Metal Foams

Nanoporous metal (NP) foams are a unique material with very high surface-to-volume ratios while maintaining the desired metallic properties. They are utilized in many different applications due to their structure including batteries [77] and catalysts [78]. It is due to the nanostructure that more efficient materials can be made in comparison to the bulk material. Rather than have a strictly ordered shape, the nanofoams would have a more diverse mixture of larger and small pores. Having many small pores would result in large surface areas which lead to more reaction areas and better capacity. With larger pore sizes there is a possibility of some increased efficiency due to better connections as the larger pores connect smaller pores.

The NP metal foams are considered a material network of pores, struts, and joints in the nanometer range. However, due to the structure, there is a limitation on the material properties that the materials can have as large freestanding films are difficult to fabricate. The idea is to attach the NP metal foams onto a polymer substrate in order to create a responsive bi-layer. By doing so, the NP metal foam is supported by the flexible substrate which can allow for deformations much larger than the film can handle by itself. These deformations allow for the tuning of the porosity of the material, which has been shown to alter properties such as electric conductivity [79].

Planar layered heterostructures have been used in research and commercial products including thermostats. In most cases, delamination, separation between the substrate and the top film, is the main failure mechanism. With a strong interface between the two materials, the structure behaves as one. The composite utilizes the difference in material properties at the interface between a base substrate and a deposited thin film to

develop a residual stress. The built-in stress will create a response when the structure is released and external excitations would affect the residual stress to elicit a different response. As the elastomer elastically deforms, it allows for tuning of the NP metal foam that cannot be accomplished just during the fabrication process. The subsequent deformation in the NP metal foam causes changes in the material property.

The different stimuli considered to trigger the response of the NP metal foam/PDMS heterostructures are temperature, solvent, and built in residual stresses. The changes in temperature are meant to expand or contract the polymer substrate. Similarly, a chemical stimulus like a solvent would cause swelling in the polymer, which would result in change of the structure/morphology of the NP metal foam. Built in residual stresses, introduced by pre-straining the polymer prior to the metal deposition, can be used to either counter or enhance the internal stresses that are generated at the interface of the two materials.

This chapter will detail the materials and methods chosen to fabricate the bi-layer structures. An approach to characterize and stimulate the planar heterostructures and determine how they react to different triggers including temperature, chemical stimuli, and locked in stresses is also presented.

The planar bi-layer heterostructures is comprised of a PDMS substrate and an Au NP foam on top. PDMS is the material of choice for the base substrate due to its relatively low modulus and ability to customize its modulus based on curing conditions and monomer to curing agent ratio. In general, the top layer film needs to have at least one physical property that is significantly different than that of the base substrate. Modulus and coefficient of thermal expansion are the two properties of interest in the PDMS/Au NP foam structure.

The manufacturing of the planar heterostructures is shown schematically in Figure 3-1 and is split up into two parts. The first part, shown in Figure 3-1a, is the fabrication method for the PDMS film. The first stage requires polyacrylic acid (PAA) deposition, PDMS deposition, and in some cases PDMS film release. The second part includes the process to prepare the pdms film prior to deposition of the NP metal foam. The steps include PDMS film stretching, metal structure deposition, and finally structure release.

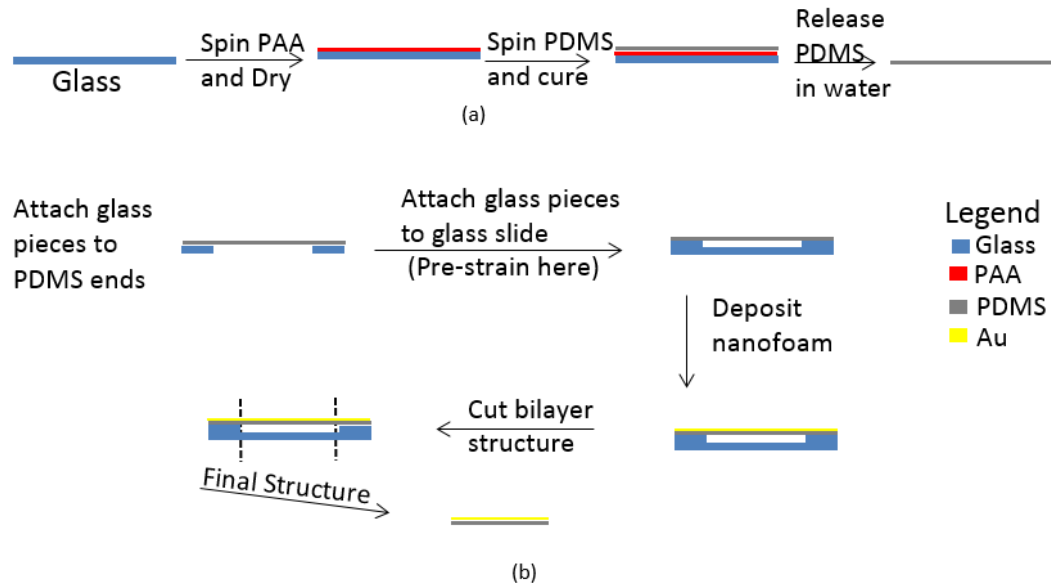


Figure 3-1: Fabrication process for polymer/foam bi-layer (a) PDMS film fabrication (b) Pre-stressed bilayer fabrication

In general, cured PDMS films will peel off of a glass slide. For very thick film fabrication, there is no need for a sacrificial layer and the films can be spun directly on a substrate such as a glass slide or a polystyrene petri dish. With very thin films, the process of peeling off the PDMS introduces the possibility of ripping the film. To eliminate the chance of ripping during the process, use of a sacrificial layer between the PDMS and the glass substrate was necessary. The choice of sacrificial layer was polyacrylic acid (PAA 50% wt Aqueous solution M.W. 5000, Acros Organics). This material is water soluble

which allows for a simple method to dissolve the sacrificial layer without affecting the PDMS substrate. A higher molecular weight PAA will result in a much thicker aqueous solution which may need to be thinned or spun faster to allow for better thickness control.

In order to maintain a uniform layer, the PAA solution was deposited through spin coating on a glass slide. For the fabrication, the PAA was spun at 1000 RPM for one minute. This layer was then placed on a hot plate at 100° c for 30 minutes to evaporate the water out of the aqueous solution. This leaves a thin film of PAA spread across the glass slide. The PAA layer thickness is inconsequential as its thickness does not come into play in the overall structure of the composite. The thinner the layer the shorter the time necessary for the PAA to be dissolved.

The PDMS was spun on top of the dried PAA layer. PDMS was set to 10:1 by weight of monomer to crosslinker ratio. Spin speed and spin duration was utilized to control the thickness of the polymer layer, with faster speeds correlating to thinner layers. The faster spin speeds also result in a more uniform layer. Longer spin times give a more uniform deposited layer with the consequence of slowly thinning out the PDMS layer. Note with spin coating, a round substrate is typically desired to keep consistent thickness. For most spins, there is an edge effect that is inherent in the process which leads to slightly thicker films on the edges.

In order to determine the appropriate conditions for the desired thickness, a variety of spin speeds were first tested followed by modifying the spin times to help with the film uniformity. Initial spin speeds were chosen from between 200-2000 RPM and spun for 1.5 minutes, guided by previous research on spun PDMS film thickness. Films were spun, released, cut, and measured to determine the nominal thickness for each spin condition.

Figure 3-2 shows the calibration curve generated from these tests, where the average thickness of a film were plotted versus the spin speed. The spin speed and spin time were chosen in order to achieve either layers of 25 and 100 μm . The final spin conditions were determined as 2000 RPM for 1.5 minute for the 25 μm thickness and 400 RPM for 3 min for the 100 μm case. The 3 min spin time was determined as additional tests with increasing spin time were used to make the layers more consistent in thickness. After spinning the PDMS layers, the polymer was cured at 80°C for 1 hr.

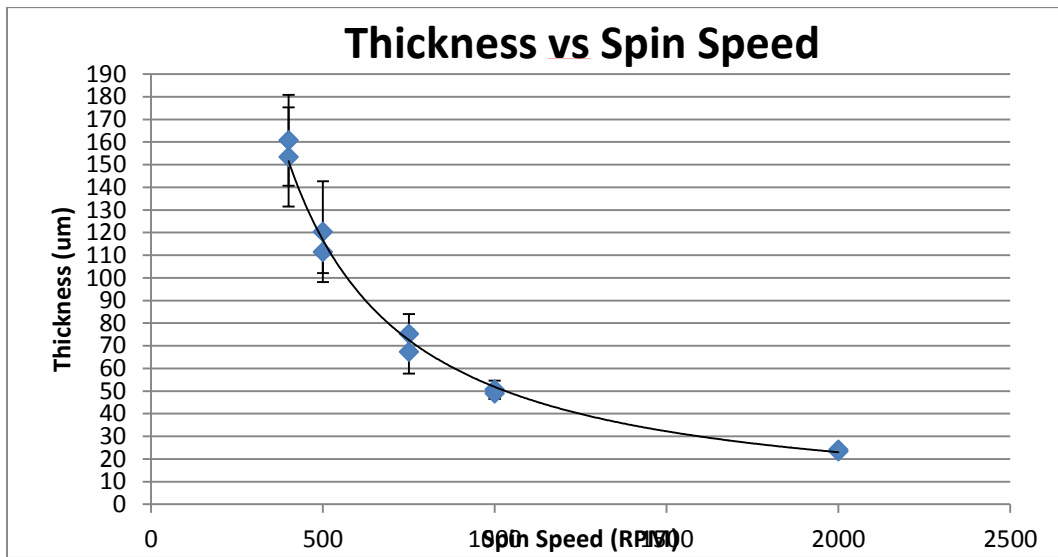


Figure 3-2: Thickness vs Spin Speed calibration curve

The films were released from the glass substrate by submersion in water so that pre-strain could be introduced prior to top layer deposition. The films were considered released when they floated in the water. They were pulled out of the water by sliding a glass slide underneath the film and then being raised up. Pulling out the full film end is meant to eliminate some of the folding that could occur when using a tweezer to pull the film out of the water. Thinner films, the 25 μm in particular, had an issue with the film end

folding in on itself when pulled out of water. This is thought to happen due to the surface tension of the water. The released films were then left to air dry.

When drying was completed, the second stage started with small pieces of glass being glued to both ends of the PDMS film to provide both a place to grip when stretching the films and places to apply glue. The film was not attached directly to a glass slide with glue because there is no control on the spread of glue during attachment. Permanent attachment was desired due to size constraints of the structure that can be put into the evaporator (that is used to deposit the metal alloy). With a mechanical structure holding the films, if the force is not evenly distributed, then the held edges will curl at the places with more force.

After the glue dried, the films were stretched manually using a ruler to record the applied strain and the glass pieces were glued down to another slide. The glass pieces used as grips need to be pulled away from each other straight as emphasis on one edge over the other would mean uneven strain. The top metal film were then deposited on top of the PDMS film through evaporation followed by dealloying. Dealloying was chosen due to its low temperature compatibility and solvent compatibility. The advantage to this method of fabrication is the interface compared to an alternate method of fabrication as a full layer is deposited onto the substrate

This fabrication method suspends the PDMS film above a glass substrate with a small air gap. The raised film fabrication allows for a simplified structure release by cutting the PDMS film.

The concern with this process is the manual stretching. With very thin films, it is possible to rip the film during the stretching process. This is especially exacerbated with

the 25um thick films that were stretched to at least 10% strain. As the glue is fast setting, the stretched pieces must be stretched prior to attachment to the secondary glass substrate. Attaching the glass pieces and then stretching the film results in the possibility of the initial setting of the glue even prior to getting to the desired length.

An alternate method to creating the bilayer is to attach a NP metal foam film on top of the PDMS substrate instead of deposit the metal alloy and perform the dealloy process. The steps from the second stage for stretching were followed. Tape to hold the films down rather than glue were used with this method. The PDMS film was then placed in an oxygen plasma environment for 10 minutes. This is required in order to oxidize the PDMS surface reducing the hydrophobicity of PDMS facilitating stronger bonding with the hydrophilic gold and stronger interface. The NP metal foam, made by dealloying metal foil in acid, is then transferred from its acid bath onto the PDMS surface. This is done by placing an absorbent paper pad underneath the floating NP metal foam to support it when taking it out of the acid. The foam is then transferred onto the plasma treated PDMS surface and the excess acid is left to dry off the surface. As before, the manual stretching issues could still occur with this method, but it uses a simpler way to place the metal on the polymer film. However, the interface may not be as strong as the interface is formed between a full and porous surface and the surface treatment is not a permanent effect indicating that the bond may not be as strong as the original method.

As a test, structures were formed with the second method with the PDMS left unreleased from its substrate prior to the foam deposition. After the NP Au foam was transferred onto the PDMS and the whole heterostructure dried, a blade was used to cut rectangles of millimeter size sides which are then released either in water (if PAA has been

used) or manually from the glass substrate. The trigger is then applied and the change in the curvature of the NP Au/PDMS is then recorded.

It is noted that the Au NP films made contained cracks and their deposition on the PDMS substrate resulted in wrinkles and folds. The presence of the cracks is due to either extended etch times or high concentration of the acid solution used during the dealloying process. Both the etching process and the technique for picking up of the Au NP metal film from the solution need to be improved before a good sample can be made. Despite the imperfections in the samples, the NP Au/PDMS heterostructures show some response, although not quantifiable, to temperature (bend when cooled from ~ 80 °C to ambient temperature) and solvent (bend when their surrounding fluid was changed from water to hexane which swells the PDMS).

Chapter 4. Conclusions and Suggestions for Future Work

In this study, different PDMS composites were fabricated and characterized to form responsive structures that were actuated through different means. The first composite was fabricated from a mixture of PDMS and iron and was demonstrated as a material for controllable microarrays. The second composite demonstrated the use of strain engineering to actuate a NP metal foam through temperature, solvents, and induced pre-stress.

4.1 Results

The work was focused on the characterization and fabrication of new materials into their desired structures. As part of this work, the changes to the material properties were reaffirmed with the fabrication of the cylinder structures. It was shown that higher concentration of filler particles resulted in higher elastic modulus. The higher concentration of particles also allowed for much larger deformation with the same magnetic force. The actuation of a bi-layer structure has been demonstrated through the use of temperature and solvent stimuli.

4.2 Future work

Magnetic microcolumns were fabricated using mold casting with the molds made using laser cutting. The next step would be to create higher aspect ratio columns and scale the diameter back down closer to 10 μm . Better laser cutting could be applied to fabricate smaller diameter holes, higher aspect ratio, and even other shapes. The size of the structure is dependent on the laser system used to fabricate the structures as the minimum dimension would be the width of the laser beam. Another way to make the high aspect ratio holes would be going back to photolithography. Rather than making holes, the idea would be to

make su8 pillars. These pillars would then be utilized to fabricate a master PDMS mold that could then be surface treated so that the elastomer micro-columns can be cast from the master mold. This would be similar to the method in [36].

In this study, only one type of material was utilized as the filler for magnetic actuation. There are many other materials that could be used to trigger a similar response, and the current particles size would need to be scaled down with progressively smaller diameter holes. In terms of the filler, pursuing anisotropy to the distribution of the particles would be a possible way to increase the efficiency of the structures. Other groups have shown structures that consolidate the metal particles in the column tip, which increases the fabrication complexity. The benefit of anisotropy will have to be balanced with any additional processing or equipment needed for proper fabrication.

A concern with the magnetic actuation used in this thesis was that using a single magnet has limitations in the field strength especially far away from the magnet. A better actuation method would be to place the structures in a uniform magnetic field, which can be possibly done with an electro magnet or u shaped magnet such that the structures would be placed between the two poles of the magnet.

An equation that relates the elastic modulus, volume fraction, magnetization, and particle size to the bend angle needs to be developed. The equation discussed in chapter 3 does not seem valid to the current system; this is most likely due to size and distribution effects with a small part being due to the structure not being high enough aspect ratio. The composite had many agglomerations, rather than uniform homogeneity, and was formed from micron sized particles rather than the derived equations nanoparticles. If these differences could be accounted for, a better equation to predict performance of the

fabricated structures would be immensely useful for design purposes. It may also help to measure the magnetization of the polymer to help confirm these predictions.

For the laminated structure, it is necessary to make a better structure so that the actuation is reversible and more pronounced. The first step would be to create better foams so that the structures are not cracked prior to and post placement on substrate. It might also be necessary to decrease the thickness of the PDMS layer. After optimization of both foam and PDMS is finished, the material properties could be then measured while being actuated. Porosity, and consequently conductivity, could be measured to show that theoretical tuning of material through actuation could be adapted.

For the bilayer composite, only one nanoporous metal foam material was deposited on the polymer substrate. As the dealloying process could be used for a variety of materials, these planar bilayers could be fabricated with other materials as a way to confirm how the actuation affects the material property.

The development of composite materials will continue on with many challenges that need to be tackled its implementation for daily use. An extension of using filler materials and a way to flexibly tune a metallic nanofoam has been demonstrated. The concern will be how to adapt this technology to larger scale processes and how to increase its efficiency.

References

- [1] B. Simpson, G. Nunnery, R. Tannenbaum, and K. Kalaitzidou, "Capture/release ability of thermo-responsive polymer particles," *Journal of Materials Chemistry*, vol. 20, pp. 3496-3501, 2010.
- [2] E. C. Peters, F. Svec, and J. M. J. Fréchet, "Thermally responsive rigid polymer monoliths," *Advanced Materials*, vol. 9, pp. 630-633, 1997.
- [3] Y.-J. Chuang, T.-H. Liao, P.-R. Chen, and K.-Y. Hung, "Experimental investigation of a display chip incorporating an electrostatic actuating polymer membrane," *Journal of Micromechanics and Microengineering*, vol. 20, p. 085020, 2010.
- [4] B. A. Evans, A. R. Shields, R. L. Carroll, S. Washburn, M. R. Falvo, and R. Superfine, "Magnetically Actuated Nanorod Arrays as Biomimetic Cilia," *Nano Letters*, vol. 7, pp. 1428-1434, 2007/05/01 2007.
- [5] Y. Wang, Y. Gao, H. Wyss, P. Anderson, and J. den Toonder, "Out of the cleanroom, self-assembled magnetic artificial cilia," *Lab on a Chip*, vol. 13, pp. 3360-3366, 2013.
- [6] L. D. Zarzar, P. Kim, and J. Aizenberg, "Bio-inspired Design of Submerged Hydrogel-Actuated Polymer Microstructures Operating in Response to pH," *Advanced Materials*, vol. 23, pp. 1442-1446, 2011.
- [7] C. L. van Oosten, C. W. M. Bastiaansen, and D. J. Broer, "Printed artificial cilia from liquid-crystal network actuators modularly driven by light," *Nat Mater*, vol. 8, pp. 677-682, 08//print 2009.
- [8] E. Cabane, X. Zhang, K. Langowska, C. Palivan, and W. Meier, "Stimuli-Responsive Polymers and Their Applications in Nanomedicine," *Biointerphases*, vol. 7, pp. 1-27, 2012/02/11 2012.
- [9] H. Meng and Jinlian Hu, "A Brief Review of Stimulus-active Polymers Responsive to Thermal, Light, Magnetic, Electric, and Water/Solvent Stimuli," *Journal of Intelligent Material Systems and Structures*, vol. 21, pp. 859-885, June 1, 2010 2010.
- [10] K. G. Neoh and E. T. Kang, "Responsive surfaces for biomedical applications," *MRS Bulletin*, vol. 35, pp. 673-681, 2010.

- [11] P. Krulevitch, A. P. Lee, P. B. Ramsey, J. C. Trevino, J. Hamilton, and M. A. Northrup, "Thin film shape memory alloy microactuators," *Microelectromechanical Systems, Journal of*, vol. 5, pp. 270-282, 1996.
- [12] W. M. Huang, B. Yang, L. An, C. Li, and Y. S. Chan, "Water-driven programmable polyurethane shape memory polymer: Demonstration and mechanism," *Applied Physics Letters*, vol. 86, pp. -, 2005.
- [13] B. Dong and Z. Li, "Cement-based piezoelectric ceramic smart composites," *Composites Science and Technology*, vol. 65, pp. 1363-1371, 7// 2005.
- [14] P. G. Mercado and A. P. Jardine, "Smart thin film TiNi/piezoelectric heterostructures," *Journal of Vacuum Science & Technology A*, vol. 13, pp. 1017-1021, 1995.
- [15] R. Samatham, I.-S. Park, K. J. Kim, J.-D. Nam, N. Whisman, and J. Adams, "Electrospun nanoscale polyacrylonitrile artificial muscle," *Smart Materials and Structures*, vol. 15, p. N152, 2006.
- [16] K. Wilde, P. Gardoni, and Y. Fujino, "Base isolation system with shape memory alloy device for elevated highway bridges," *Engineering Structures*, vol. 22, pp. 222-229, 3// 2000.
- [17] F. Liu and M. W. Urban, "Recent advances and challenges in designing stimuli-responsive polymers," *Progress in Polymer Science*, vol. 35, pp. 3-23, 1// 2010.
- [18] H. Meng and G. Li, "A review of stimuli-responsive shape memory polymer composites," *Polymer*, vol. 54, pp. 2199-2221, 4/19/ 2013.
- [19] A. Moisala, Q. Li, I. A. Kinloch, and A. H. Windle, "Thermal and electrical conductivity of single- and multi-walled carbon nanotube-epoxy composites," *Composites Science and Technology*, vol. 66, pp. 1285-1288, 8// 2006.
- [20] S.-F. Wang, Y.-R. Wang, K.-C. Cheng, and Y.-P. Hsaio, "Characteristics of polyimide/barium titanate composite films," *Ceramics International*, vol. 35, pp. 265-268, 1// 2009.
- [21] H. Ishida and S. Rimdusit, "Very high thermal conductivity obtained by boron nitride-filled polybenzoxazine," *Thermochimica Acta*, vol. 320, pp. 177-186, 11/2/ 1998.

- [22] M. Riahi and E. Alizadeh, "Fabrication of a 3D active mixer based on deformable Fe-doped PDMS cones with magnetic actuation," *Journal of Micromechanics and Microengineering*, vol. 22, p. 115001, 2012.
- [23] Y. Xia and G. M. Whitesides, "SOFT LITHOGRAPHY," *Annual Review of Materials Science*, vol. 28, pp. 153-184, 1998.
- [24] M. J. Madou, *Fundamentals of Microfabrication: The Science of Miniaturization, Second Edition*: Taylor & Francis, 2002.
- [25] G. J. Schmitz, C. Brücker, and P. Jacobs, "Manufacture of high-aspect-ratio micro-hair sensor arrays," *Journal of Micromechanics and Microengineering*, vol. 15, p. 1904, 2005.
- [26] A. Grimes, D. N. Breslauer, M. Long, J. Pegan, L. P. Lee, and M. Khine, "Shrinky-Dink microfluidics: rapid generation of deep and rounded patterns," *Lab on a Chip*, vol. 8, pp. 170-172, 2008.
- [27] B. A. Evans, B. L. Fiser, W. J. Prins, D. J. Rapp, A. R. Shields, D. R. Glass, *et al.*, "A highly tunable silicone-based magnetic elastomer with nanoscale homogeneity," *Journal of Magnetism and Magnetic Materials*, vol. 324, pp. 501-507, 2// 2012.
- [28] M. C. Petty, "Electroactive Organic Compounds," in *Molecular Electronics*, ed: John Wiley & Sons, Ltd, 2007, pp. 169-211.
- [29] B. L. Gray, "A Review of Magnetic Composite Polymers Applied to Microfluidic Devices," *Journal of The Electrochemical Society*, vol. 161, pp. B3173-B3183, January 1, 2014 2014.
- [30] N. Dempsey, "Hard Magnetic Materials for MEMS Applications," in *Nanoscale Magnetic Materials and Applications*, J. P. Liu, E. Fullerton, O. Gutfleisch, and D. J. Sellmyer, Eds., ed: Springer US, 2009, pp. 661-683.
- [31] W. Wang, Z. Yao, J. C. Chen, and J. Fang, "Composite elastic magnet films with hard magnetic feature," *Journal of Micromechanics and Microengineering*, vol. 14, p. 1321, 2004.

- [32] C.-Y. Chen, C.-Y. Chen, C.-Y. Lin, and Y.-T. Hu, "Magnetically actuated artificial cilia for optimum mixing performance in microfluidics," *Lab on a Chip*, vol. 13, pp. 2834-2839, 2013.
- [33] M. Rahbar, S. Seyfollahi, A. Khosla, B. L. Gray, and L. Shannon, "Fabrication Process for Electromagnetic Actuators Compatible with Polymer Based Microfluidic Devices," *ECS Transactions*, vol. 41, pp. 7-17, May 4, 2012 2012.
- [34] A. Khosla, J. L. Korčok, B. L. Gray, D. B. Leznoff, J. W. Herchenroeder, D. Miller, *et al.*, "Fabrication and testing of integrated permanent micromagnets for microfluidic systems," 2010, pp. 759316-759316-8.
- [35] Z. Varga, G. Filipcsei, and M. Zrínyi, "Magnetic field sensitive functional elastomers with tuneable elastic modulus," *Polymer*, vol. 47, pp. 227-233, 01 / 03 / 2006.
- [36] F. Khademolhosseini and C. Mu, "Fabrication and Patterning of Magnetic Polymer Micropillar Structures Using a Dry-Nanoparticle Embedding Technique," *Microelectromechanical Systems, Journal of*, vol. 22, pp. 131-139, 2013.
- [37] E. Suhir, "Interfacial Stresses in Bimetal Thermostats," *Journal of Applied Mechanics*, vol. 56, pp. 595-600, 1989.
- [38] V. Y. Prinz, V. A. Seleznev, V. A. Samoylov, and A. K. Gutakovsky, "Nanoscale engineering using controllable formation of ultra-thin cracks in heterostructures," *Microelectronic Engineering*, vol. 30, pp. 439-442, 1// 1996.
- [39] M. Huang, C. Boone, M. Roberts, D. E. Savage, M. G. Lagally, N. Shaji, *et al.*, "Nanomechanical Architecture of Strained Bilayer Thin Films: From Design Principles to Experimental Fabrication," *Advanced Materials*, vol. 17, pp. 2860-2864, 2005.
- [40] O. G. Schmidt and K. Eberl, "Nanotechnology: Thin solid films roll up into nanotubes," *Nature*, vol. 410, pp. 168-168, 03/08/print 2001.
- [41] S. Huang and X. Zhang, "Gradient residual stress induced elastic deformation of multilayer MEMS structures," *Sensors and Actuators A: Physical*, vol. 134, pp. 177-185, 2/28/ 2007.

- [42] J.-Y. Sun, S. Xia, M.-W. Moon, K. H. Oh, and K.-S. Kim, "Folding wrinkles of a thin stiff layer on a soft substrate," *Proceedings of the Royal Society A: Mathematical, Physical and Engineering Science*, November 23, 2011 2011.
- [43] X. Feng, Y. Huang, and A. J. Rosakis, "On the Stoney Formula for a Thin Film/Substrate System With Nonuniform Substrate Thickness," *Journal of Applied Mechanics*, vol. 74, pp. 1276-1281, 2007.
- [44] Y. Zhang and Y.-p. Zhao, "Applicability range of Stoney's formula and modified formulas for a film/substrate bilayer," *Journal of Applied Physics*, vol. 99, pp. -, 2006.
- [45] B. Simpson, "Strain Engineering as a method for Manufacturing Micro & Nanoscale Responsive Particles," M.S., Mechanical Engineering, Georgia Tech, 2010.
- [46] A. K. Geim, S. V. Dubonos, I. V. Grigorieva, K. S. Novoselov, A. A. Zhukov, and S. Y. Shapoval, "Microfabricated adhesive mimicking gecko foot-hair," *Nat Mater*, vol. 2, pp. 461-463, 07//print 2003.
- [47] Y. Liu, J. Tang, R. Wang, H. Lu, L. Li, Y. Kong, *et al.*, "Artificial lotus leaf structures from assembling carbon nanotubes and their applications in hydrophobic textiles," *Journal of Materials Chemistry*, vol. 17, pp. 1071-1078, 2007.
- [48] H. U. Riisgard and P. S. Larsen, "Minireview: Ciliary filter feeding and bio-fluid mechanics-- present understanding and unsolved problems," *Limnology and Oceanography*, vol. 46, pp. 882-891, 2001.
- [49] C. Jorgensen, T. Kiorboe, F. Mohlenberg, and H. Riisgard, "Ciliary and mucus-net filter feeding, with special reference to fluid mechanical characteristics," *Mar. Ecol. Prog. Ser.*, vol. 15, pp. 283-292, 1984.
- [50] L. J. Fauci and R. Dillon, "BIOFLUIDMECHANICS OF REPRODUCTION," *Annual Review of Fluid Mechanics*, vol. 38, pp. 371-394, 2006/01/01 2005.
- [51] P. Satir and S. T. Christensen, "Overview of Structure and Function of Mammalian Cilia," *Annual Review of Physiology*, vol. 69, pp. 377-400, 2007.
- [52] B. A. Evans, "Design, Fabrication, and Actuation of Biomimetic Cilia," PHD, Physics, University of North Carolina at Chapel Hill, NC, 2008.

- [53] F. G. Barth, *A Spider's World: Senses and Behavior*: Springer, 2002.
- [54] J. D. Toonder, F. Bos, D. Broer, L. Filippini, M. Gillies, J. De Goede, *et al.*, "Artificial cilia for active micro-fluidic mixing," *Lab on a Chip - Miniaturisation for Chemistry and Biology*, vol. 8, pp. 533-541, 01 / 01 / 2008.
- [55] F. Fahrni, M. W. J. Prins, and L. J. Van Ijzendoorn, "Micro-fluidic actuation using magnetic artificial cilia," *Lab on a Chip - Miniaturisation for Chemistry and Biology*, vol. 9, pp. 3413-3421, 01 / 01 / 2009.
- [56] K. Oh, J.-H. Chung, S. Devasia, and J. J. Riley, "Bio-mimetic silicone cilia for microfluidic manipulation," *Lab on a Chip*, vol. 9, pp. 1561-1566, 2009.
- [57] J. Belardi, N. Schorr, O. Prucker, and J. R uhe, "Artificial Cilia: Generation of Magnetic Actuators in Microfluidic Systems," *Advanced Functional Materials*, vol. 21, pp. 3314-3320, 2011.
- [58] B. Pokroy, A. K. Epstein, M. C. M. Persson-Gulda, and J. Aizenberg, "Fabrication of Bioinspired Actuated Nanostructures with Arbitrary Geometry and Stiffness," *Advanced Materials*, vol. 21, pp. 463-469, 2009.
- [59] J. V. I. Timonen, C. Johans, K. s. Kontturi, A. Walther, O. Ikkala, and R. H. A. Ras, "A Facile Template-Free Approach to Magnetodriven, Multifunctional Artificial Cilia," *ACS Applied Materials & Interfaces*, vol. 2, pp. 2226-2230, 2010/08/25 2010.
- [60] M. Ballard, Z. Mills, S. Beckworth, and A. Alexeev, "Enhancing nanoparticle deposition using actuated synthetic cilia," *Microfluidics and Nanofluidics*, pp. 1-8, 2013/12/19 2013.
- [61] H. Masoud and A. Alexeev, "Harnessing synthetic cilia to regulate motion of microparticles," *Soft Matter*, vol. 7, pp. 8702-8708, 2011.
- [62] A. Bhattacharya, G. A. Buxton, O. B. Usta, and A. C. Balazs, "Propulsion and Trapping of Microparticles by Active Cilia Arrays," *Langmuir*, vol. 28, pp. 3217-3226, 2012/02/14 2012.
- [63] R. Ghosh, G. A. Buxton, O. B. Usta, A. C. Balazs, and A. Alexeev, "Designing Oscillating Cilia That Capture or Release Microscopic Particles," *Langmuir*, vol. 26, pp. 2963-2968, 2010/02/16 2009.

- [64] C. Semmler and A. Alexeev, "Designing structured surfaces that repel fluid-borne particles," *Physical Review E*, vol. 84, p. 066303, 12/05/ 2011.
- [65] J. Branscomb and A. Alexeev, "Designing ciliated surfaces that regulate deposition of solid particles," *Soft Matter*, vol. 6, pp. 4066-4069, 2010.
- [66] B. C. Tappan, S. A. Steiner, and E. P. Luther, "Nanoporous Metal Foams," *Angewandte Chemie International Edition*, vol. 49, pp. 4544-4565, 2010.
- [67] Y. Jiang, S. Yang, Z. Hua, and H. Huang, "Sol–Gel Autocombustion Synthesis of Metals and Metal Alloys," *Angewandte Chemie International Edition*, vol. 48, pp. 8529-8531, 2009.
- [68] Z. Hua, Y. Deng, K. Li, and S. Yang, "Low-density nanoporous iron foams synthesized by sol-gel autocombustion," *Nanoscale Research Letters*, vol. 7, pp. 1-7, 2012/02/14 2012.
- [69] N. Leventis, N. Chandrasekaran, C. Sotiriou-Leventis, and A. Mumtaz, "Smelting in the age of nano: iron aerogels," *Journal of Materials Chemistry*, vol. 19, pp. 63-65, 2009.
- [70] N. Leventis, N. Chandrasekaran, A. G. Sadekar, C. Sotiriou-Leventis, and H. Lu, "One-Pot Synthesis of Interpenetrating Inorganic/Organic Networks of CuO/Resorcinol-Formaldehyde Aerogels: Nanostructured Energetic Materials," *Journal of the American Chemical Society*, vol. 131, pp. 4576-4577, 2009/04/08 2009.
- [71] B. C. Tappan, M. H. Huynh, M. A. Hiskey, D. E. Chavez, E. P. Luther, J. T. Mang, *et al.*, "Ultralow-Density Nanostructured Metal Foams: Combustion Synthesis, Morphology, and Composition," *Journal of the American Chemical Society*, vol. 128, pp. 6589-6594, 2006/05/01 2006.
- [72] K. Zhang, X. Tan, J. Zhang, W. Wu, and Y. Tang, "Template-dealloying synthesis of ultralow density Au foams with bimodal porous structure," *RSC Advances*, vol. 4, pp. 7196-7201, 2014.
- [73] I. Vukovic, S. Punzhin, Z. Vukovic, P. Onck, J. T. M. De Hosson, G. ten Brinke, *et al.*, "Supramolecular Route to Well-Ordered Metal Nanofoams," *ACS Nano*, vol. 5, pp. 6339-6348, 2011/08/23 2011.

- [74] J. Biener, A. M. Hodge, J. R. Hayes, C. A. Volkert, L. A. Zepeda-Ruiz, A. V. Hamza, *et al.*, "Size Effects on the Mechanical Behavior of Nanoporous Au," *Nano Letters*, vol. 6, pp. 2379-2382, 2006/10/01 2006.
- [75] R. Liu and A. Antoniou, "A relationship between the geometrical structure of a nanoporous metal foam and its modulus," *Acta Materialia*, vol. 61, pp. 2390-2402, 4// 2013.
- [76] I. T. GABE, J. H. GAULT, J. ROSS, D. T. MASON, C. J. MILLS, J. P. SCHILLINGFORD, *et al.*, "Measurement of Instantaneous Blood Flow Velocity and Pressure in Conscious Man with a Catheter-Tip Velocity Probe," *Circulation*, vol. 40, pp. 603-614, November 1, 1969 1969.
- [77] S. Zhang, Y. Xing, T. Jiang, Z. Du, F. Li, L. He, *et al.*, "A three-dimensional tin-coated nanoporous copper for lithium-ion battery anodes," *Journal of Power Sources*, vol. 196, pp. 6915-6919, 8/15/ 2011.
- [78] J. Snyder, T. Fujita, M. W. Chen, and J. Erlebacher, "Oxygen reduction in nanoporous metal-ionic liquid composite electrocatalysts," *Nat Mater*, vol. 9, pp. 904-907, 11//print 2010.
- [79] W. Zhou, Y. Tang, R. Song, L. Jiang, K. S. Hui, and K. N. Hui, "Characterization of electrical conductivity of porous metal fiber sintered sheet using four-point probe method," *Materials & Design*, vol. 37, pp. 161-165, 5// 2012.